A&A 565, A112 (2014)
DOI: 10.1051/0004-6361/201323340

Astronomy & Astrophysics

New light on gamma-ray burst host galaxies with *Herschel*⋆,⋆⋆

L. K. Hunt[1], E. Palazzi[2], M. J. Michałowski[3,4,⋆⋆⋆,⋆⋆⋆⋆], A. Rossi[2,5], S. Savaglio[6,7], S. Basa[8], S. Berta[6], S. Bianchi[1], S. Covino[9], V. D'Elia[10,11], P. Ferrero[12], D. Götz[13], J. Greiner[6], S. Klose[5], D. Le Borgne[14], E. Le Floc'h[13], E. Pian[2], S. Piranomonte[11], P. Schady[6], and S. D. Vergani[15,9]

[1] INAF – Osservatorio Astrofisico di Arcetri, Largo E. Fermi 5, 50125 Firenze, Italy
e-mail: hunt@arcetri.astro.it
[2] INAF – IASF Bologna, via Gobetti 101, 40129 Bologna, Italy
[3] Sterrenkundig Observatorium, Universiteit Gent, Krijgslaan 281-S9, 9000 Gent, Belgium
[4] SUPA, Institute for Astronomy, University of Edinburgh, Royal Observatory, Edinburgh EH9 3HJ, UK
[5] Thüringer Landessternwarte Tautenburg, Sternwarte 5, 07778 Tautenburg, Germany
[6] Max-Planck-Institut für Extraterrestrische Physik, Giessenbachstraße, 85748 Garching bei München, Germany
[7] Physics Department, University of Calabria, via P. Bucci, 87036 Rende (CS), Italy
[8] Aix-Marseille Université, CNRS, LAM (Laboratoire d'Astrophysique de Marseille) UMR 7326, 13388 Marseille, France
[9] INAF/Osservatorio Astronomico di Brera, via Emilio Bianchi 46, 23807 Merate (LC), Italy
[10] ASI Science Data Centre, via Galileo Galilei, 00044 Frascati (RM), Italy
[11] INAF – Osservatorio Astronomico di Roma, via di Frascati 33, 00040 Monteporzio Catone, Italy
[12] Instituto de Astrofísica de Andalucía (IAA-CSIC), Glorieta de la Astronomia s/n, 1008 Granada, Spain
[13] Laboratoire AIM-Paris-Saclay, CEA/DSM/Irfu – CNRS – Université Paris Diderot, CE-Saclay, pt courrier 131, 91191 Gif-sur-Yvette, France
[14] Institut d'Astrophysique de Paris, UMR 7095, CNRS, UPMC Univ. Paris 06, 98bis boulevard Arago, 75014 Paris, France
[15] GEPI-Observatoire de Paris, CNRS UMR 8111, Univ. Paris-Diderot, 5 place Jules Jannsen, 92190 Meudon, France

Received 26 December 2013 / Accepted 13 February 2014

ABSTRACT

Until recently, dust emission has been detected in very few host galaxies of gamma-ray bursts (GRBHs). With *Herschel*, we have now observed 17 GRBHs up to redshift $z \sim 3$ and detected 7 of them at infrared (IR) wavelengths. This relatively high detection rate (41%) may be due to the composition of our sample which at a median redshift of 1.1 is dominated by the hosts of dark GRBs. Although the numbers are small, statistics suggest that dark GRBs are more likely to be detected in the IR than their optically bright counterparts. Combining our IR data with optical, near-infrared, and radio data from our own datasets and from the literature, we have constructed spectral energy distributions (SEDs) which span up to 6 orders of magnitude in wavelength. By fitting the SEDs, we have obtained stellar masses, dust masses, star-formation rate (SFR), and extinctions for our sample galaxies. We find that GRBHs are galaxies that tend to have a high specific SFR (sSFR), and like other star-forming galaxies, their ratios of dust-to-stellar mass are well correlated with sSFR. Dust masses of GRBHs relative to stellar mass and SFR fall within the range of other star-forming galaxies in the local universe, and of sub-millimeter galaxies (SMGs) and luminous IR galaxies for redshift $z \gtrsim 1$. We incorporate our *Herschel* sample into a larger compilation of GRBHs, after checking for consistency in mass and SFR estimations. This combined sample is compared to SFR-weighted median stellar masses of the widest, deepest galaxy survey to date in order to establish whether or not GRBs can be used as an unbiased tracer of cosmic comoving SFR density (SFRD) in the universe. In contrast with previous results, this comparison shows that GRBHs are medium-sized galaxies with relatively high sSFRs, as might be expected for galaxies selected on the basis of SFR because of the explosive GRB event. Stellar masses and sSFRs of GRBHs as a function of redshift are similar to what is expected for star-forming galaxy populations at similar redshifts. We conclude that there is no strong evidence that GRBs are biased tracers of SFRD; thus they should be able to reliably probe the SFRD to early epochs.

Key words. galaxies: high-redshift – galaxies: star formation – galaxies: ISM – dust, extinction – submillimeter: galaxies

1. Introduction

Long-duration gamma-ray bursts (GRBs) are so luminous that they can shine through highly obscured galaxies (e.g., Djorgovski et al. 2001) and can be seen even at very high redshifts (Salvaterra et al. 2009; Tanvir et al. 2009; Cucchiara et al. 2011). They are thought to originate in the collapse of very massive stars at the end of their evolution (Paczynski 1998; MacFadyen & Woosley 1999; Woosley & Heger 2006). Because of this association with massive stars, GRBs have recently been used, thanks to the advent of the dedicated mission *Swift*, to infer the cosmic evolution of the star formation rate density (SFRD) up to $z \sim 9$ (Yüksel et al. 2008; Kistler et al. 2009; Butler et al. 2010; Robertson & Ellis 2012; Elliott et al. 2012; Trenti et al. 2013).

⋆ *Herschel* is an ESA space observatory with science instruments provided by European-led Principal Investigator consortia and with important participation from NASA.
⋆⋆ Appendix is available in electronic form at http://www.aanda.org
⋆⋆⋆ FWO Pegasus Marie Curie Fellow.
⋆⋆⋆⋆ Scottish Universities Physics Alliance.

Although GRBs are rare events, they enable identification of galaxies that would not otherwise be singled out even in deep flux-limited surveys, thus making GRBs a potentially powerful probe of galaxy evolution. Galaxies hosting GRBs (GRBHs) are better known in the low-z regime ($z \lesssim 1.5$), where they are typically low-mass, young, star-forming blue galaxies with low dust extinction (Le Floc'h et al. 2003; Christensen et al. 2004; Fruchter et al. 2006; Savaglio et al. 2009). However, these galaxy characteristics, possibly related to a selection bias because of the consideration of only optically bright GRB afterglows, may not be so uniform at high redshift. Indeed, evidence is mounting that the GRBH population is much more diverse at $z \gtrsim 1.5$ than previously thought.

Dark GRBs, those for which the observed optical afterglow is very faint relative to the extrapolation from the X-ray (Jakobsson et al. 2004; van der Horst et al. 2009), tend to be found in massive, star-forming galaxies with red colors, high extinction and large star formation rates (SFRs; e.g., Krühler et al. 2011; Rossi et al. 2012; Perley et al. 2013). Dark GRBs comprise up to 30–40% of the *Swift* GRB dataset (Fynbo et al. 2009; Greiner et al. 2011; Melandri et al. 2012), and thus the assumption that all GRBHs are low-mass, metal poor galaxies may be an oversimplification. Consequently, theoretical work based on this assumption using GRBHs as cosmological probes (Campisi et al. 2009; Niino et al. 2011; Robertson & Ellis 2012) could be undermined.

Until recently, statistics on dark GRBs and their host galaxies have been poor (e.g., Kann et al. 2010). Because of their optical faintness, it has been very difficult to localize the optical afterglow of dark GRBs, and thus identify the host (e.g., Rossi et al. 2012). Now, thanks to sustained observational efforts, we have a considerably better understanding of dark GRBs and their host galaxies. In most dark GRBs, the optical faintness is caused by high dust extinction columns and moderate redshift (Perley et al. 2009; Greiner et al. 2011; Krühler et al. 2011; Rossi et al. 2012; Melandri et al. 2012; Covino et al. 2013). However, the properties of dust extinction are not the same for all GRBs, although there is no clear evidence that afterglow extinction curves differ significantly from those commonly used (Perley et al. 2008; Zafar et al. 2011, 2012; Schady et al. 2012). It is thus difficult to make conclusive statements about the nature of GRB hosts (e.g., D'Elia 2013; Elliott et al. 2013); it is neither true that all massive, metal-rich GRBHs are found from dark GRBs (e.g., Le Floc'h et al. 2002), nor do all dark GRBs reside in massive hosts at high redshift.

Direct observations of the entire spectral energy distribution (SED) of dark GRBHs would help to place them in the context of other high-z galaxy populations, especially since the most common understanding of the high-z universe is based on optically-selected (rest-frame UV) galaxy surveys. So far, only a handful of GRBHs have been detected with sub-millimeter (submm) facilities (Barnard et al. 2003; Berger et al. 2003; Tanvir et al. 2004; Priddey et al. 2006; Wang et al. 2012; Michałowski et al. 2014). However, in this minority SFRs can be high, $\sim 500\,M_\odot$ yr^{-1}, as high as those of the submm galaxy (SMG) population (Chapman et al. 2004; Greve et al. 2005) even though the galaxies picked out by the two selection criteria are quite different. There has been no CO emission found in any of the GRBHs observed so far (e.g., Hatsukade et al. 2011) and there is some hint that dust in GRBHs may be warmer than in typical ultra-luminous infra-red galaxies (ULIRGs) and SMGs (Priddey et al. 2006; Michałowski et al. 2008).

To better understand the properties of dark GRB hosts, and to assess their potential impact on the GRBH population in general, we undertook an observational campaign with *Herschel*; this paper presents results from this campaign. We characterize the dust content, stellar mass, and SFRs of GRBHs through *Herschel* observations of 17 GRBHs, 14 of which host dark GRBs. This is the first time that *Herschel* has been used to examine dust in GRBHs; dust emission is detected in seven of our targets. Sample selection is described in Sect. 2, and Sect. 3 reports the *Herschel* observations and the other data incorporated in the compilation of the SEDs, together with the procedures for the photometry. SED fitting is discussed in Sect. 4, and Sect. 5 gives the results of the fitting in terms of stellar masses, dust masses, SFRs, and dust extinction. The properties of our sample of GRBHs are compared with other GRBH samples and other high-z star-forming galaxy populations in Sect. 6. Throughout the paper, we assume a $\Omega_m = 0.3$, $\Omega_\Lambda = 0.7$ cosmology, with Hubble constant $H_0 = 70$ km s^{-1} Mpc^{-1}.

2. Sample selection

The *Herschel* target list is based on 118 GRBHs imaged with *Spitzer*/IRAC (InfraRed Array Camera, Fazio et al. 2004), available in June 2010. We retrieved these images from the *Spitzer* archive, and when available, we also retrieved images at 24 μm acquired with *Spitzer*/MIPS (Multiband Imaging Photometer, Rieke et al. 2004). Both sets of images were reduced with MOPEX (Makovoz & Marleau 2005), taking into account the difference between the older IRAC images and those acquired with warm *Spitzer*. After having performed photometry on the images for this parent sample, we defined the *Herschel* observing sample by requiring that the host galaxy be detected in at least two *Spitzer* bands (usually IRAC). To ensure detection with *Herschel*, based on normal galaxy SEDs we estimated that the IRAC 3.6 μm or 4.5 μm flux needed to be $\gtrsim$10 μJy, so selected only the galaxies that fulfilled this flux limit. Finally, we avoided targets in crowded fields, so that the *Herschel* photometry would not be contaminated by extraneous objects near the hosts.

We thus obtained a sample of 17 GRBHs, which were observed over both (OT1 and OT2) *Herschel* observing cycles. An additional host observed in OT1, GRB 980425, the closest GRBH at $z = 0.0085$, is discussed by Michałowski et al. (2014). In OT1, we included both optically bright and dark GRBs, while in OT2, the targets were required to be the hosts of dark GRBs; dark bursts thus comprise the bulk of our sample (14 of 17 targets host dark GRBs). Throughout the paper, we define a dark GRB as one that optically falls short of the prediction of the fireball model, namely with an optical-to-X-ray spectral index $\beta_{ox} < 0.5$ (Jakobsson et al. 2004). Table 1 gives the host-galaxy positions and redshifts of the *Herschel* targets. Redshifts range from $z = 0.21$ (GRB 050219A) to $z = 3$ (GRB 090404); the median redshift $z_{med} = 1.1$. The uncertainties in the GRBH positions are $\lesssim$0.″5 in all cases.

3. The data and the photometry

We have acquired *Herschel* (Pilbratt et al. 2010) PACS and SPIRE maps for the 17 GRBHs in our observing sample, and combined them with our own data and with data from the literature to compile SEDs for GRB host galaxies that span almost 3 orders of magnitude in wavelength.

3.1. Herschel observations

Through two open-time observing programs (OT1_lhunt_2 and OT2_lhunt_3) we obtained images at 100 and 160 μm with

Table 1. Host galaxy sample.

GRB	RA (J2000)[b]	Dec	Redshift	Redshift reference[c]	Dark?[a]	Observing ID PACS	SPIRE
970828	18:08:31.56	+59:18:51.2	0.958	1	Yes	1342258609,10	1342241152
980613	10:17:57.9	+71:27:26.3	1.097	2	No	1342270864,65	–
980703	23:59:06.67	+08:35:06.7	0.966	3	No	–	1342212419
990705	05:09:54.50	−72:07:53.0	0.842	4	No	1342261814,15	1342214749
020127	08:15:01.42	+36:46:33.9	1.9[d]	5	Yes	1342243296,97	1342251906
020819B	23:27:19.52	+06:15:53.2	0.411	6	Yes	1342246708,09	1342212294
030115	11:18:32.63	+15:02:59.9	2.0[e]	7	Yes	1342247632,33	–
050219A	11:05:39.07	−40:41:04.6	0.2115	8	Yes	1342248286,87	1342247261
050223	18:05:32.99	−62:28:18.8	0.584	9	Yes	1342243788,89	1342214756
051022	23:56:04.1	+19:36:24.1	0.807	6	Yes	1342238085,86	1342247985
060904A	15:50:54.56	+44:59:10.5	2.55[d]	11	Yes	1342261849,50	–
070306	09:52:23.3	+10:28:55.5	1.496	12	Yes	1342254142,43[f]	–
071021	22:42:34.31	+23:43:06.5	2.452	13	Yes	1342246178,79	1342258356
080207	13:50:03.01	+07:30:07.8	2.086	13	Yes	1342257547,48	1342261526
080325	18:31:34.3	+36:31:24.8	1.78	14	Yes	1342245672,73	1342241156
090404	15:56:57.52	+35:30:57.5	3.00[d]	14	Yes	1342258433,34	1342241163
090417B	13:58:46.66	+47:01:04.4	0.345	15	Yes	1342257593,94	1342259467

Notes. [(a)] These GRBs are classified as dark according to the definitions by Jakobsson et al. (2004); van der Horst et al. (2009). [(b)] These are the positions of the host galaxy, which may or may not be exactly coincident with the position of the GRB afterglow. [(c)] (1) Djorgovski et al. (2001); (2) Djorgovski et al. (2003); (3) Djorgovski et al. (1998); (4) Le Floc'h et al. (2002); (5) Berger et al. (2007); (6) Levesque et al. (2010b); (7) Levan et al. (2006); (8) Rossi et al. (2014); (9) Pellizza et al. (2006); (10) Chary et al. (2007); (11) Xiao & Schaefer (2011); (12) Jaunsen et al. (2008); (13) Krühler et al. (2012); (14) Perley et al. (2013); (15) Holland et al. (2010). [(d)] Photometric redshift. [(e)] Photometric redshift determined by our GRASIL fits. [(f)] Although this source was in our target list, this observation was acquired in the OT2 proposal, OT2_ppschady_2.

PACS (Photodetector Array Camera & Spectrometer[1], Poglitsch et al. 2010) and at 250, 350, and 500 μm with SPIRE (Spectral and Photometric Imaging REceiver[2], Griffin et al. 2010).

We used PACS in Small-Scan map mode (20″/s), with 10 scan legs, 3′ long, separated by 4″ steps. The scans were divided into two Astronomical Observation Requests (AORs), with orthogonal scan directions which were executed sequentially (see Table 1). With this configuration we obtain homogeneous coverage over an area with a diameter of ∼2′, sufficient to cover the region subtended by the hosts. Cross scans gave the needed redundancy to avoid $1/f$ noise and spurious detector glitches on science and noise maps. The estimated 1σ sensitivity is 0.5 mJy at 100 μm and 1.7 mJy at 160 μm. With SPIRE in Small-Map Mode, we used 4 repetitions in order to obtain a sensitivity of roughly the 1σ confusion limit (see Nguyen et al. 2010) of ∼6 mJy beam^{-1} at 250 μm. SPIRE observations were obtained only for a subset of the observations.

Data reduction for PACS and SPIRE was performed with HIPE (*Herschel* Imaging Processing Environment; Ott 2010) v10.0. For PACS, the "deep survey point-source" option was used, with masking performed on the images themselves before combining the repetitions and orthogonal scans into a single map. We used pixel sizes of 2.″0 and 3.″0 for PACS 100, 160 μm, and 4.″5, 6.″25 and 9.″0 for SPIRE 250, 350, and 500 μm, respectively. These pixels well sample the PACS and SPIRE full-width half-maximum beam sizes of ∼6.″8 and 11.″4 (for PACS 100 and 160 μm), and 18.″2, 24.″9, and 36.″3 (for SPIRE 250, 350, and 500 μm, respectively). With the aim of maximizing sensitivity to extended emission, we also reduced the PACS data with `scanamorphos` (Roussel 2013). However, the slightly larger reconstructed beam resulted in overall worse noise characteristics although flux levels did not differ significantly with the previous reduction. Hence, we used the photometry from the deep-survey reduction mode.

3.2. Herschel photometry

We checked the astrometry of the *Herschel* images using astrometry of USNO stars in the field, and translated the *Herschel* images when necessary to be consistent with the *Spitzer*/IRAC astrometry. In each PACS and SPIRE image, an estimate for the background was obtained by averaging the flux measured within a set of empty sky apertures close to the galaxies. After background subtraction, the flux densities of the entire host galaxy at all *Herschel* wavelengths were obtained in apertures of radius 6″, except for the host of GRB 020819B for which we used an aperture of radius 13″. This larger aperture was used because of the large angular size of the GRB 020819B host (Levesque et al. 2010b). Following the PACS calibration guidelines[3], we adjusted the photometry for the appropriate aperture correction, and corrected the uncertainty estimates for correlated noise. Color corrections are around unity within the uncertainties, so we neglected them. The uncertainties associated with the measured photometry were computed as a combination in quadrature of the calibration uncertainty, 7% for SPIRE data (according to Version 2.4, 2011 June 7, of the SPIRE Observer's Manual)

[1] PACS has been developed by a consortium of institutes led by MPE (Germany) and including UVIE (Austria); KU Leuven, CSL, IMEC (Belgium); CEA, LAM (France); MPIA (Germany); INAF-IFSI/OAA/OAP/OAT, LENS, SISSA (Italy); IAC (Spain). This development has been supported by the funding agencies BMVIT (Austria), ESA-PRODEX (Belgium), CEA/CNES (France), DLR (Germany), ASI/INAF (Italy), and CICYT/MCYT (Spain).

[2] SPIRE has been developed by a consortium of institutes led by Cardiff University (UK) and including Univ. Lethbridge (Canada); NAOC (China); CEA, LAM (France); IFSI, Univ. Padua (Italy); IAC (Spain); Stockholm Observatory (Sweden); Imperial College London, RAL, UCL-MSSL, UKATC, Univ. Sussex (UK); and Caltech, JPL, NHSC, Univ. Colorado (USA). This development has been supported by national funding agencies: CSA (Canada); NAOC (China); CEA, CNES, CNRS (France); ASI (Italy); MCINN (Spain); SNSB (Sweden); STFC, UKSA (UK); and NASA (USA).

[3] These are found at the URL: `http://herschel.esac.esa.int/twiki/bin/view/Public/PacsCalibrationWeb#PACS_calibration_and_performance`

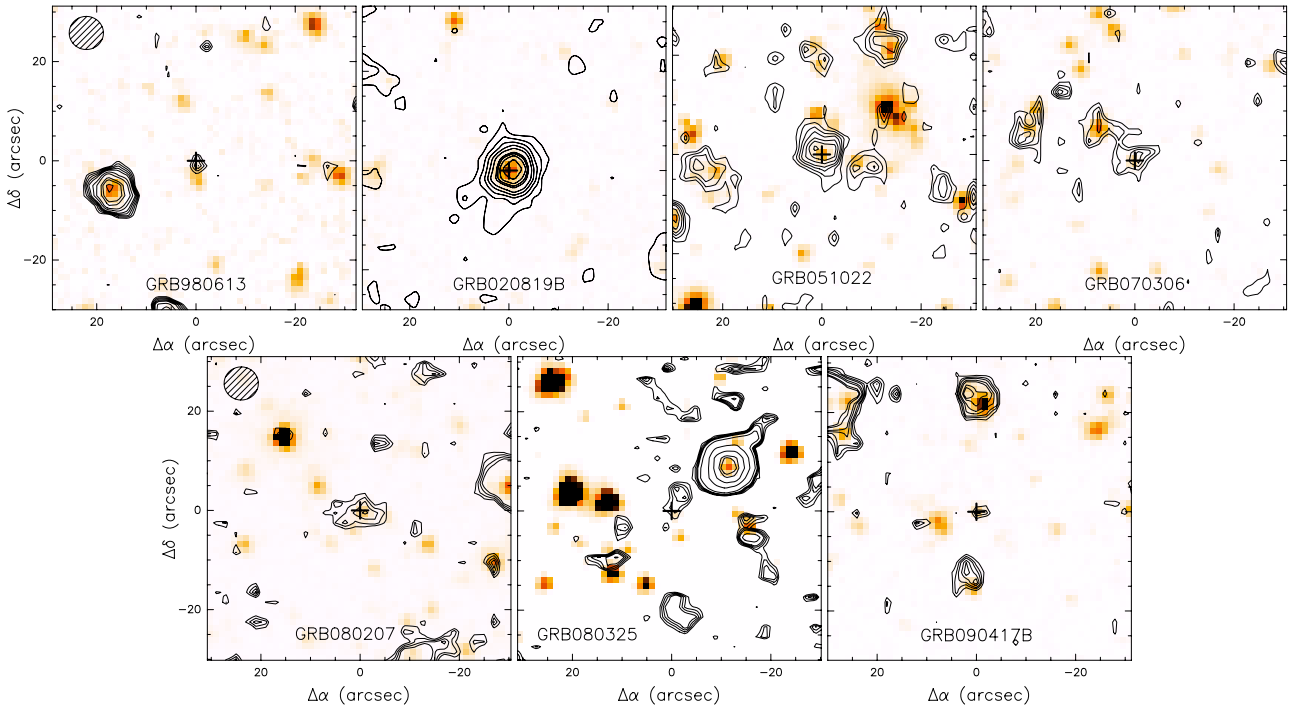

Fig. 1. PACS 100 μm images of the 7 detected galaxies superimposed as contours on the *Spitzer*/IRAC 3.6 μm images shown with false colors (for the host of GRB 980613, the IRAC 4.5 μm is plotted). The (0, 0) position corresponds to the coordinates given in Table 1. The slight vertical offsets in the various panels result from inability to perfectly center the IRAC images because of the integer pixels. The PACS 100 μm beam size is shown in the upper left corner of the left-most panel in each row. PACS contours start at 3σ and run to 4.5σ (980613), 30σ (020819B), 7σ (051022), 6σ (070306), 6σ (080207), 3.5σ (080325), and 5σ (090417B). These σ values per pixel correspond to the correlated noise measured from the images, which are roughly 4 times smaller than the true noise (see PACS documentation and text). A + marks the nominal GRBH position (see Table 1). The detection of the host of GRB 080325 is only marginal, significant at ~2.5σ. For display purposes, the PACS images have been rebinned to smaller pixel sizes.

and 5% for PACS data (according to Version 2.3, 2011 June 8 of the PACS Observer's Manual), and the sky uncertainty derived by considering the number of pixels of the given aperture and the standard deviation of the average value in the individual sky apertures. Before addition in quadrature, the sky uncertainties were corrected for the correlated noise, since the pixels are not independent. The *Herschel* photometry and its uncertainties are given in Appendix A, Table A.1.

We detect 7 GRBHs with *Herschel* at redshifts ranging from z = 0.35–2.1; all of these detections are PACS, but GRBH 020819B (z = 0.4) also has SPIRE detections. Figure 1 shows the PACS 100 μm images for the 7 detections overlaid on IRAC images (3.6 μm except for the host of GRB 980613 which is 4.5 μm). The (0, 0) position corresponds to the host coordinates reported in Table 1, and is marked by a +. The host of GRB 080325 has only a marginal detection, significant at ~2.5σ.

3.3. Other multiwavelength data

To complete the SEDs, we gathered broadband optical, near-infrared, millimeter and centimeter portions of the SED from our own datasets or from the literature. In particular, we obtained new optical/near-infrared data for the hosts of GRBs 050219A and 050223 with the Gamma-Ray burst Optical and Near-infrared Detector (GROND; Greiner et al. 2008). These data were reduced in a standard manner, using mainly the GROND pipeline (Yoldaş et al. 2008; Krühler et al. 2008). Aperture photometry was performed by using an aperture twice the diameter of the full-width half-maximum of the stellar point-spread function (PSF).

As described in Sect. 2, we retrieved the infrared data for all the hosts in our sample from the *Spitzer* archive, and reduced the available IRAC and MIPS data with MOPEX (Makovoz & Marleau 2005). We then performed photometry on these images using a small circular aperture with a radius of 4″ (~5–7 times the IRAC PSF), with background subtraction determined from empty sky regions around the source. Aperture corrections have been applied only in a few cases (the hosts of GRBs 020127, 020819B, 050219A, and 080207), in order to take into account their extension relative to the small apertures. For the IRAC images of GRBH 090404, because of the possible contamination from the nearby galaxies (see Perley et al. 2013), we applied the procedure described by Molinari et al. (2011) to extract the host fluxes.

Radio and submm data were taken from Berger et al. (2001), Berger et al. (2003), Tanvir et al. (2004), Stanway et al. (2010), de Ugarte Postigo et al. (2012), Hatsukade et al. (2012), Svensson et al. (2012), Perley & Perley (2013). The photometry used for the SED fitting is reported in Table A.1, together with additional references.

4. Fitting the spectral energy distributions

We have used the multiwavelength dataset described in the previous section to estimate the dust masses, stellar masses, and SFRs in the sample GRBHs. For the first time, we are able to place constraints on the dust emission in a significant sample of GRBHs. Before fitting the SED, photometry was corrected for Galactic extinction assuming the values of A_V taken from the NASA Extragalactic Database, (NED, `http://ned.ipac.`

caltech.edu), and using the interstellar extinction curve by Cardelli et al. (1989).

We applied the SED fitting method introduced by Michałowski et al. (2009, 2010) based on 35 000 templates in the library of Iglesias-Páramo et al. (2007), plus additional templates of Silva et al. (1998) and Michałowski et al. (2008), all developed in GRASIL[4] (Silva et al. 1998). They are based on numerical calculations of radiative transfer within a galaxy, which is assumed to be a triaxial system with diffuse dust and dense molecular clouds that are the sites of star formation. A discussion of the derivation of galaxy properties and typical uncertainties is given by Michałowski et al. (2009).

The templates cover a broad range of galaxy properties from quiescent to starburst. Their star formation histories (SFHs) are assumed to be a smooth Kennicutt-Schmidt (KS)-type law (SFR proportional to the gas mass to some power, see Silva et al. 1998, for details) with a starburst (if any) on top of that starting 50 Myr before the current epoch at that redshift. There are seven free parameters in the library of Iglesias-Páramo et al. (2007): the normalization of the KS law, the timescale of the mass infall, the intensity of the starburst, the timescale of the molecular cloud destruction, the optical depth of molecular clouds, the age of the galaxy and the inclination of the disk with respect to the observer. These templates are based on a Salpeter (Salpeter 1955) initial mass function (IMF), but in the analysis the stellar masses and SFRs have been converted to a Chabrier (2003) IMF by dividing by a factor of 1.8.

4.1. Uncertainties on the fitted parameters

SED fitting procedures are notoriously degenerate (e.g., Le Borgne & Rocca-Volmerange 2002), especially when estimating photometric redshifts (as in GRB 030115, see Table 1). We have therefore run a series of tests to establish the realistic uncertainties on the various parameters determined by GRASIL. These tests have shown that the stellar masses are formally good to within 40%, but comparison with other templates (see Sect. 5.1 below) suggests that a factor of 2 may be more realistic when comparing with other samples. The stellar portion of the SED for our hosts is usually well constrained, but stellar masses tend to differ according to the adopted SFHs (see Michałowski et al. 2012a). SFR values (both UV, IR) are accurate to roughly 30%, and the burst masses to within a factor of 2. The dust masses have an uncertainty of ~0.3 dex (a factor of 2), and the dust temperature 10−20 K, or even more because of the sparse sampling of the SED around its peak.

4.2. Modified blackbody fits

In order to obtain realistic upper limits to the dust mass, in the cases where GRASIL models were unable to do so because of non-detections, we also fit single-temperature modified blackbodies (MBBs) to the IR SED using PACS upper limits. Such fits assume that the dust is optically thin, with an emissivity that varies as a power law, with index β. These are very simplistic fits, in which we attempted only to derive the maximum dust mass that would pass through the data points. The MBB emissivity index β was fixed to 2 (e.g., Bianchi 2013), and the temperature was fixed to $T = 35 \pm 1$ K (e.g., Michałowski et al. 2008, 2010). The dust mass was calculated using the Milky Way dust opacities given by Draine & Li (2007). The upper limit to the dust mass was taken to be the inferred total dust mass calculated at 160 μm. In only one case, the host of GRB 060904A, is the GRASIL approximation of the non-detections more realistic. We repeated the procedure also for the detected GRBHs, and find agreement with the GRASIL values to within a factor of 2. Hence, the MBB upper limits are expected to be compatible with GRASIL, and can be analyzed in a coherent way.

[4] http://www.adlibitum.oat.ts.astro.it/silva

5. Results

Figure 2 shows the best-fit GRASIL models of the 17 GRBH multiwavelength SEDs. Table 2 reports the best-fit parameters given by GRASIL. In the cases where there is no *Herschel* detection (see Col. 6 of Table 2), the dust masses are intended to be upper limits (as noted by <). Column 11 of Table 2 gives the resulting $M_{\rm dust}$ for the MBB fitting as described in Sect. 4.2. These are intended only as very approximate upper limits to the dust mass, given the flux limits implied by our *Herschel* observations. The values of A_V given by the GRASIL fits are an average over the entire galaxy, and take into account the total attenuation given by the extinction in the diffuse interstellar medium (ISM) combined with that in the dense molecular clouds (see Silva et al. 1998).

Unlike GRB samples that are selected in order to be as statistically unbiased as possible (Fynbo et al. 2009; Greiner et al. 2011; Hjorth et al. 2012; Salvaterra et al. 2012), our sample of GRBHs is not a statistically complete sample in any sense. Nevertheless, because our sample is dominated by hosts of dark GRBs (14/17), it is unique and, in combination with other samples from the literature (e.g., Savaglio et al. 2009; Perley et al. 2013)[5], can give a new perspective on the characterization of the galaxy masses, dust content, and SFR of the long-GRBH population. After comparing our results with previous work, in the following sections we compare the stellar masses, dust masses, SFRs, and host extinctions of the combined sample with other galaxy populations covering a similar redshift interval. We postpone the discussion of trends of stellar mass and SFR with redshift to Sect. 6.

5.1. Comparison with previous work

Because of the lack of detections at IR or sub-mm wavelengths (e.g., Berger et al. 2003; Tanvir et al. 2004; Priddey et al. 2006), dust masses have been determined for very few GRB hosts before now (e.g., Michałowski et al. 2008). The dust mass for one of our *Herschel* targets, GRBH 980703, was also calculated by Michałowski et al. (2008), and our fit here is very similar to that found with earlier data (no IR detections then or now), giving virtually identical limits to the dust mass.

Stellar masses can be compared more readily. Six galaxies in our sample have been studied by Savaglio et al. (2009) or Castro Cerón et al. (2010), and 12 are in common with Perley et al. (2013). To estimate stellar masses, Castro Cerón et al. (2010) uses rest-frame K-band luminosities with an approximate mass-to-light ratio; correcting both mass estimates to a Chabrier (2003) IMF gives a mean ratio of dex(−0.21) $M_\odot$, with our masses being ~1.6 times smaller than theirs. Savaglio et al. (2009) use SED fitting to the rest-frame optical and UV photometry, and consider two star-formation episodes; their stellar masses are, in the mean, 2.5 times smaller than ours, perhaps because of the lack of *Spitzer*/IRAC data which could be important for our dark-GRB dominated sample. Perley et al. (2013)

[5] In the Savaglio et al. (2009) sample, as noted before, we have eliminated from further consideration the hosts of 6 short GRBs studied therein.

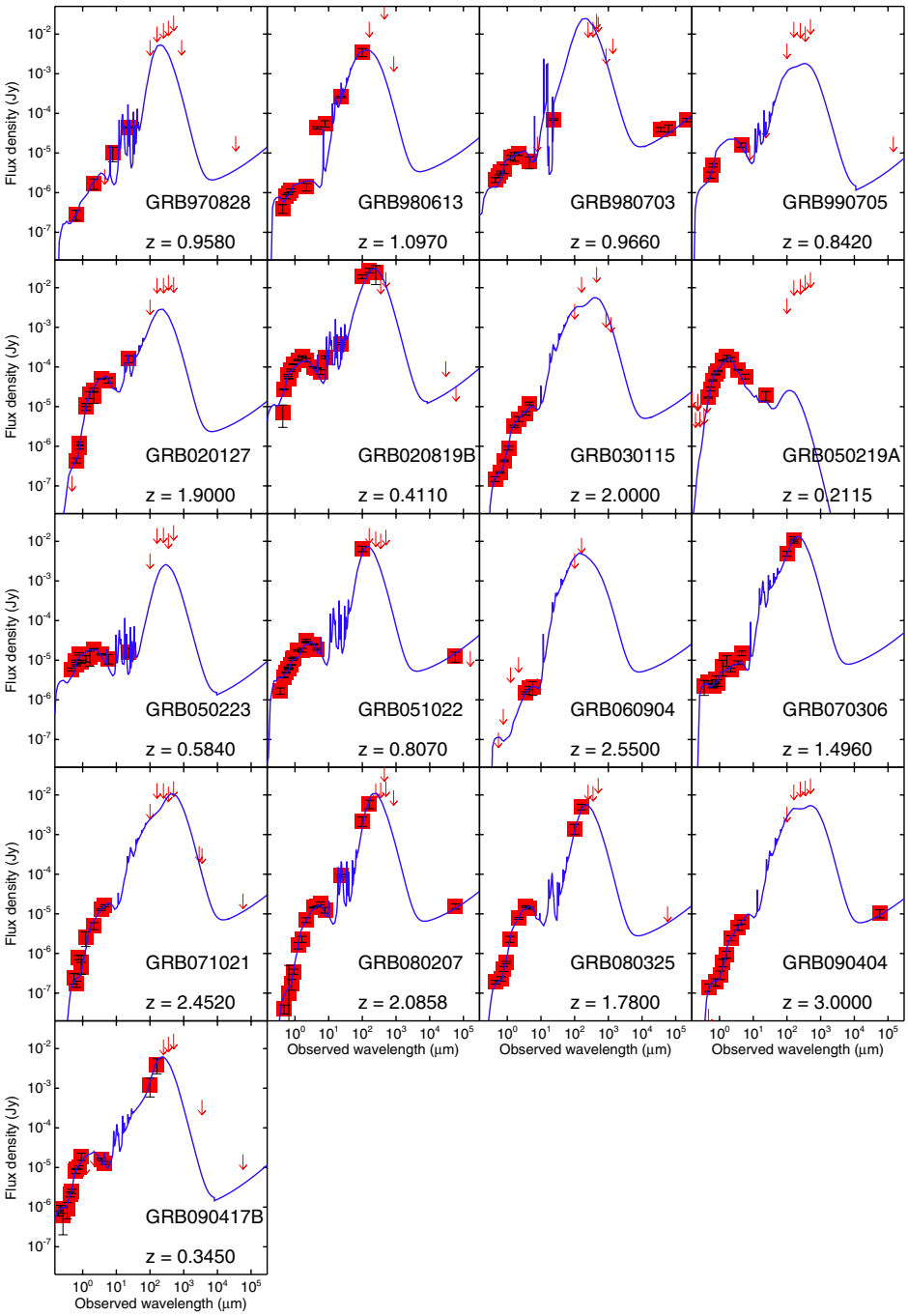

Fig. 2. Best-fitting GRASIL models in Jy plotted against wavelength, superimposed on the multiwavelength data for the GRBHs. Upper limits are shown as downward arrows where the head of the arrow indicates the 3σ upper limit.

use SED fitting with a single episode of star formation, but include *Spitzer*/IRAC data where possible. Our estimates of stellar masses are, on average, 1.7 times larger than theirs, with a large standard deviation. One possible cause of this difference is that GRASIL uses a two-episode SFH which tends to give larger stellar masses than estimates based on one star-formation episode (Michałowski et al. 2012a). The biggest discrepancy is for the host of GRB 980613, for which the estimate by Castro Cerón et al. (2010) is roughly 40 times larger than ours, and ~200 times larger than the one given by Perley et al. (2013). This could be due to the complex configuration of this host, which consists of at least five galaxies, or galaxy fragments (Djorgovski et al. 2003). In general, the scatter among all the comparisons is ~dex(0.4–0.6), or roughly a factor of 3. Given the different approaches and the different sets of photometry, this could be considered reasonable agreement, and probably a realistic estimate of the uncertainty.

The comparison of the stellar masses of the 20 galaxies (not in our sample) common to Savaglio et al. (2009) and Perley et al. (2013) show very good agreement between these two studies, with a mean difference of dex(0.03) and a standard deviation between the two sets of measurements of dex(0.4), or a factor of ~2.5. We consider this to be good agreement, and in what follows will include both samples in our analysis when possible.

We have compared our SFRs to those found by Savaglio et al. (2009), Castro Cerón et al. (2010) and Perley et al. (2013), and find similar agreement. Again, correcting all SFR estimates to the Chabrier (2003) IMF, we find that our estimates

Table 2. GRASIL fitting results.

GRB host galaxy	SFR(UV)[a] ($M_\odot$ yr^{-1})	SFR(IR)[a] ($M_\odot$ yr^{-1})	A_V (mag)	log L_{IR} ($L_\odot$)	*Herschel* detected?	log M^a_{stars} ($M_\odot$)	log M^a_{burst} ($M_\odot$)	log M_{dust} ($M_\odot$)	T_{dust} (GRASIL) (K)	Modified blackbody fits log(M_{dust}) ($M_\odot$)
(1)	(2)	(3)	(4)	(5)	(6)	(7)	(8)	(9)	(10)	(11)
970828	0.3	14.4	2.38	11.18	No	9.80	8.96	–	38.7	<8.21
980613	1.5	39.5	1.94	11.62	Yes	9.31	9.28	7.53	71.5	–
980703	2.7	86.4	1.94	11.96	No	9.98	9.60	–	38.7	<8.65
990705	2.3	6.6	0.16	10.84	No	10.50	–	–	28.5	<8.18
020127	2.7	56.3	0.39	11.77	No	11.51	9.54	–	61.3	<9.01
020819B	3.5	13.0	0.54	11.13	Yes	10.52	–	8.99	24.4	–
030115	1.6	159.1	1.95	12.22	No	10.87	9.85	–	33.2	<9.53
050219A	<0.1	<0.1	0.00	8.29	No	9.91	–	–	47.2	<6.37
050223	1.9	1.7	0.21	10.25	No	10.02	–	–	21.0	<7.87
051022	4.8	17.9	0.56	11.27	Yes	10.29	9.28	7.27	52.6	–
060904A	1.1	303.9	4.17	12.50	No	10.18	10.17	<8.41	132.0	–
070306	9.6	144.1	1.65	12.18	Yes	10.05	9.97	8.29	52.6	–
071021	2.6	288.2	1.72	12.48	No	11.40	10.15	–	33.2	<9.50
080207	1.0	170.1	1.69	12.25	Yes	11.17	10.16	8.15	61.3	–
080325	1.2	66.5	1.03	11.84	Yes	11.09	9.62	8.06	52.6	–
090404	3.1	380.8	2.28	12.60	No	11.10	10.30	–	52.6	<9.93
090417B	0.2	1.7	0.54	10.25	Yes	9.73	–	8.18	21.0	–

Notes. [(a)] The SFRs and stellar masses have been converted to a Chabrier (2003) IMF by dividing by a factor of 1.8. Column (2): SFR inferred from SED fitting and rest-frame UV, uncorrected for extinction; Col. (3): SFR inferred from the IR emission from radiation reprocessed by dust; Col. (4): total A_V obtained by considering the total attenuation in both the diffuse ISM and the dense molecular cloud components as described in the text; Col. (5): total IR luminosity from dust emission; Col. (7): total stellar mass of the galaxy; Col. (8): stellar mass of the burst episode assumed to have onset 50 Myr ago; Col. (9): total dust mass of the galaxy; Col. (10): luminosity-weighted mean dust temperature as given by GRASIL; Col. (11): the fixed-temperature ($T = 35 \pm 1$ K) fixed-emissivity ($\beta = 2.0$) MBB fits are given when the GRASIL fit does not give a realistic upper limit.

from the UV, SFR(UV), are, in the mean, within a few percent of those by Castro Cerón et al. (2010) (with a spread of roughly a factor of 2). Because neither the GRASIL SFR(UV)s nor the Castro Cerón et al. (2010) estimates have been corrected for extinction, this good agreement is probably an indication that extinction corrections are the biggest stumbling block for consistent UV-derived SFRs.

The comparison with GRASIL SFRs estimated from the IR, SFR(IR), is less straightforward. It is well known that IR-inferred SFRs can be much larger than those derived from fitting the UV continuum (e.g., Berger et al. 2003; Buat et al. 2010). For our sample, the mean ratio of SFR(IR)/SFR(UV) given by the GRASIL fits is ∼16. For the 12 galaxies in common with Perley et al. (2013), their SFRs are on average ∼8 times larger than the GRASIL UV-based SFRs (uncorrected for extinction) and roughly half the IR SFRs given by our GRASIL fits. For the six galaxies in common with Savaglio et al. (2009), the GRASIL SFR(UVs) are ∼3 times smaller than theirs and the SFR(IR) ∼3 times larger. Given the different methods used to derive SFRs (emission lines, SED fitting), such discrepancies are not unexpected. The SFRs given by Savaglio et al. (2009) and Perley et al. (2013) lie between the SFR(IR) and SFR(UV) extremes, although their greater similarity with SFR(IR) from GRASIL implies that careful SED multiwavelength fitting with reasonable assumptions for the SFH can partially compensate the lack of IR or sub-mm data. We conclude that the SFRs we obtain here are reasonable estimates, and in what follows we will adopt the IR-derived SFRs enabled by our *Herschel* observations.

5.2. Ages and star-formation histories of GRBHs

The GRASIL fits give us some idea of what the SFH of the hosts has been. In particular, we can understand if a recent burst of star formation (over the last ∼50 Myr, see Sect. 4) has contributed significantly to the stellar mass budget, or whether most of the stars have been created over longer timescales. In Fig. 3, we plot against specific SFR (sSFR, SFR/M_{star}) the ratio of mass produced by the recent starburst episode M_{burst} and the total stellar mass in the galaxy, M_{star}. The SFR considered in the sSFR is that inferred by GRASIL from the IR luminosity and corresponds to the star formation over the last several hundreds of Myr, rather than the most recent burst. Although the quantities in the two axes are highly correlated, the comparison shows that the SFH calculated by GRASIL is realistic, or at least self-consistent with the SFR and M_{star}.

Figure 3 illustrates the expected result that the hosts with the highest sSFR also have a significant fraction of their stellar mass produced in a recent burst; half the galaxies in the observed sample have ≳10% of their stellar mass from such an episode. There is clearly a trend of M_{burst}/M_{star} with sSFR; the four galaxies with the highest ratio are also those with s$SFR \gtrsim 10^{-8}$ yr^{-1}, and would be considered starbursts at any redshift (at least $z \lesssim 3$, e.g., Elbaz et al. 2011). These are also among the galaxies with the least pronounced rest-frame 1.6 μm photometric bump (see Fig. 2) generally associated with evolved stellar populations. Because of increased stellar opacities, the strength of this bump increases with age and metallicities (Simpson & Eisenhardt 1999; Sawicki 2002), so a weak 1.6 μm feature signifies young age or sub-solar metallicity (or both). Because of the correlation we find between M_{burst}/M_{star} and sSFR, we attribute the weakness of this bump in the hosts of GRBs 980613, 980703, 060904A, and 070306 to young ages, although these galaxies may be relatively metal poor as well.

Interestingly, the *Herschel* detections are not uniquely associated with high sSFRs (≳10^{-8} yr^{-1}). Of the four shown in Fig. 3 only GRBHs 980613 and 070306 are detected with PACS.

The GRBH with the lowest sSFR (∼10^{-11} yr^{-1}) is the host of GRB 050219A (see also Fig. 3), and it is also the galaxy with

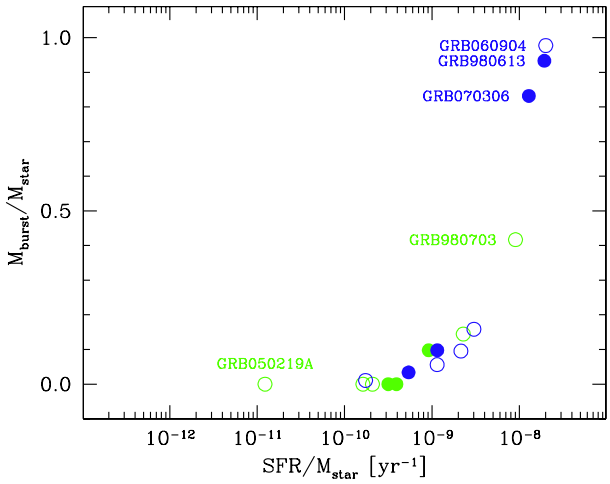

Fig. 3. Ratio of stellar mass in burst M_{burst} to total stellar mass M_{star} vs. specific SFR. *Herschel* detections are shown with filled symbols, and non-detections with open ones; blue symbols correspond to GRBHs with $z > 1.1$ (z_{med}) and green ones to GRBHs with $z \leq 1.1$. The most extreme hosts are labeled by the GRB name.

the smallest amount of dust and the lowest SFR (see Table 2). This galaxy is peculiar for a host of a long GRB, and will be discussed in a future paper (Rossi et al. 2014).

5.3. Stellar masses and SFR

We explore in Fig. 4 sSFR vs. M_{star}, or the "main sequence" (MS) of star formation (e.g., Salim et al. 2007; Noeske et al. 2007). To augment the GRBH statistics, in this and subsequent figures when possible, we have included the 23 hosts identified with *Swift* GRBs and the 31 pre-*Swift* ones studied by Perley et al. (2013), together with the hosts of 40 *long* mostly optically bright GRBs studied by Savaglio et al. (2009). These numbers do not exclude the galaxies in common with our study (see Sect. 6 for a fuller discussion). In the rest of the paper, where there are duplicates, we will prefer our values of M_{star} and SFR, then those of Perley et al. (2013), except where the quality of the fit is poor, as given by reduced $\chi^2_\nu \leq 4$; in this case we take the parameters from Savaglio et al. (2009). This order of preference is dictated by the inclusion of longer-wavelength data points in the SED fitting; even though the agreement between these two data sets is quite good (see Sect. 5.1), Perley et al. (2013) is preferred over the Savaglio et al. (2009) values because of the inclusion of *Spitzer*/IRAC data.

The left panel of Fig. 4 shows our sample as (green, blue for $z \leq z_{med}$, $z > z_{med}$, respectively) circles, and galaxies from Perley et al. (2013) as filled (magenta) diamonds and from Savaglio et al. (2009) as filled (magenta) squares; the right panel adds other galaxy populations from $z \sim 0$ to $z \gtrsim 3$. The host of GRB 980425 (Michałowski et al. 2014) is shown as a (cyan) asterisk; its extremely low redshift ($z = 0.0085$) makes it unique among GRBHs. The curves in Fig. 4 report the trends for the star-formation MS fitted by Karim et al. (2011) for $z \sim 0$, $z \sim 1$, and $z \sim 2$ (from lower curve to the upper one).

It is clear from the figure that the GRBHs span a wide range in sSFRs, and the most extreme objects have very high sSFRs, similar to or even more extreme than the Lyman-break galaxies (LBGs) at $z \sim 3$. As expected, because higher-than-average sSFRs tend to be associated with lower-than-average stellar masses, such GRBHs are not the most massive. The comparison with other galaxy populations and the trends of sSFR and M_{star} expected with redshift illustrated by the curves in Fig. 4 suggest that the GRBHs studied here are medium-size high-sSFR galaxies, as might be expected for galaxies selected on the basis of SFR because of the explosive GRB event.

5.4. Dust, stars, and SFR

Up to now, dust emission has been detected in very few GRBHs (Berger et al. 2003; Tanvir et al. 2004; Priddey et al. 2006; Wang et al. 2012; Le Floc'h et al. 2012; Michałowski et al. 2014). Pre-*Swift* studies showed a $\gtrsim 3\sigma$ detection rate at 850 μm of 2/26 hosts, ~8% (Tanvir et al. 2004). Moreover, the blue colors of these brightest hosts at submm wavelengths (e.g., GRB 000418, GRB 010222: Le Floc'h et al. 2003; Gorosabel et al. 2003) are not typical of galaxy populations selected in submm surveys. Of 15 GRBHs around $z \sim 1$, only three were detected at 24 μm with *Spitzer* (GRB 970828, GRB 980613, GRB 990705: Le Floc'h et al. 2006). These low detection rates of dust emission in GRBHs combined with measurements of stellar mass and UV-inferred SFRs (e.g., Savaglio et al. 2009) led to the conclusion that the host population was biased against dusty, massive and strongly starbursting galaxies, at least for $z \lesssim 1.5$.

Over the last few years, however, evidence has emerged that GRBHs are a more diverse population than previous work suggested. Prompt follow-up observations have enabled the localization of afterglows in a significant percentage of dark GRBs (e.g., Greiner et al. 2011; Melandri et al. 2012; Hjorth et al. 2012), thus opening the possibility of studying their hosts. With our *Herschel* observations, we have detected dust emission in 7 of 17 GRBHs, 6 of which host dark GRBs. For dark GRBs alone, the detection rate is quite high, 6/14 (43%). The detection rate for hosts of optically bright afterglows is lower (1/4, 25%), and since these are small numbers, the rate of optically bright host detections could be considered consistent with the previous, low, IR detection rates. Although the statistics are sparse, the fractions suggest that the hosts of dark GRBs are more likely to be detected at IR/submm wavelengths than their optically bright counterparts.

Recent work has shown that in star-forming galaxies M_{star}, M_{dust}, and SFR are mutually correlated (e.g., da Cunha et al. 2010b). Figure 5 shows ratios of M_{dust}/M_{star} plotted against M_{star} (in the left panel) and against sSFR (in the right). There is very little correlation between M_{dust}/M_{star} and M_{star}, but M_{dust}/M_{star} and sSFR are strongly correlated with dust-to-stellar mass ratios increasing with sSFR. A similar trend was found by da Cunha et al. (2010b) for a sample of star-forming galaxies selected from the Sloan Digital Sky Survey (SDSS), with a requirement of 60 and 100 μm detections from the Infrared Astronomical Satellite. The three curves in the right panel Fig. 5 correspond to the MS of star formation given by Karim et al. (2011, and shown in Fig. 4), but incorporating the regression of M_{dust} with SFR found by da Cunha et al. (2010b)[6]. The vertical trend of the $z \sim 2$ (dot-dashed) curve results from the fall-off of the sSFR at high stellar masses at that redshift.

Interestingly, the correlation between M_{dust} and SFR (and M_{dust}/M_{star} and sSFR) found by da Cunha et al. (2010b) overestimates dust mass relative to stellar mass at high sSFR

[6] $M_{dust}\,(M_\odot) = (1.28 \times 2.02) \times 10^7\,(SFR\,(M_\odot\ yr^{-1})^{1.11})$ where we have multiplied the da Cunha et al. (2010b) normalization by a factor of 2.02 to correct their (lower) dust masses to the GRASIL scale because of differences in the assumed dust emissivity.

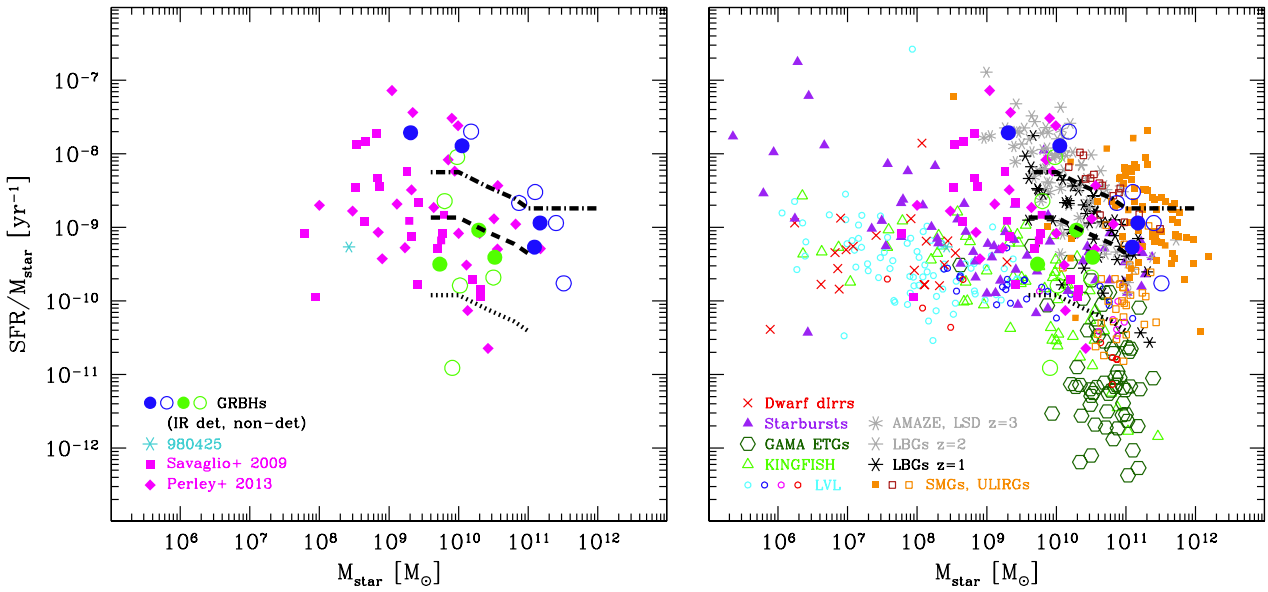

Fig. 4. Specific SFR plotted against stellar mass: the *left panel* shows GRBHs only and the *right panel* includes other galaxy populations. The three curves are the fits to the star-formation MS at $z = 0.2–0.4$ (dotted lower line), $z = 1.0–1.2$ (dashed middle), and $z = 2.0–2.5$ (dot-dashed upper) by Karim et al. (2011). The GRBHs observed by *Herschel* are indicated by filled (for IR detections) and open (IR non-detections) circles; blue symbols correspond to GRBHs with $z > 1.1$ (median z of the sample), and green ones to GRBHs with $z \leq 1.1$. GRBHs from Perley et al. (2013); Savaglio et al. (2009, excluding duplicates with our sample) are shown as filled (magenta) diamonds and as filled (magenta) squares, respectively. The host of GRB 980425 is shown with (cyan) 6-pronged asterisks (Michałowski et al. 2014). Star-forming galaxies at $z \sim 0$ from the KINGFISH sample are shown as open (light green) triangles (Kennicutt et al. 2011) and GAMA early-type galaxies (ETGs) from Rowlands et al. (2012) by open (dark green) hexagons. The parameters for the other $z \sim 0$ galaxy populations have been taken from Hunt et al. (2012) with galaxies in the Local Volume Legacy (LVL) survey shown as open circles, color-coded for Hubble type (red are early types, cyan are late types); dwarf irregular galaxies at $z \sim 0$ are shown as (red) ×; starbursts at $z \sim 0$ as (purple) filled triangles. $z \sim 2$ SMGs and $z \sim 1–2$ ULIRGs from Michałowski et al. (2010) and Lo Faro et al. (2013) are given by (orange) filled and open squares, respectively; (firebrick) open squares correspond to $z \sim 0$ ULIRGs from da Cunha et al. (2010a). Lyman-break galaxies (LBGs) at $z \sim 1$ and $z \sim 2$ are indicated by 6-pronged asterisks (Shapley et al. 2004, 2005; Oteo et al. 2013a,b); LBGs at $z \sim 3$ by 8-pronged asterisks (Maiolino et al. 2008; Mannucci et al. 2009).

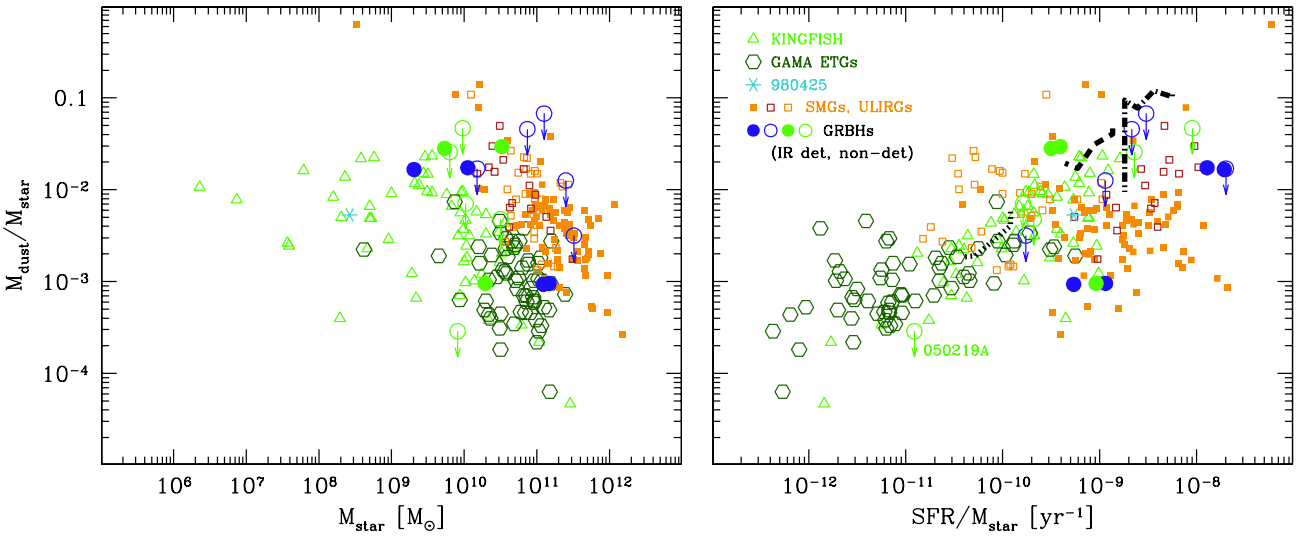

Fig. 5. Ratio of $M_{\rm dust}/M_{\rm star}$ plotted against stellar mass $M_{\rm star}$ (*left panel*) and against SFR/$M_{\rm star}$ sSFR (*right*). As in Fig. 4, the GRBHs observed by *Herschel* are indicated by filled (for IR detections) and open (IR non-detections) circles, and the other galaxy samples shown are also coded as in Fig. 4. The three curves in the *right panel* are the fits of sSFR vs. $M_{\rm star}$ at $z = 0.2–0.4$ (dotted lower), $z = 1.0–1.2$ (dashed middle), and $z = 2.0–2.5$ (dot-dashed upper) by Karim et al. (2011), as shown in Fig. 4, but here incorporating the dependence of $M_{\rm dust}$ on SFR as found at $z \approx 0$ by da Cunha et al. (2010b). The vertical trend of the $z \sim 2$ curve is related to the fall-off of sSFR at high stellar masses (see Fig. 4).

(see also da Cunha et al. 2010a); this is probably not surprising since the correlation was calibrated in the Local Universe where such extremes are rare. As seen also in Fig. 4, Fig. 5 shows that GRBHs tend toward high sSFR, and occupy the same region in parameter space as local ULIRGs (da Cunha et al. 2010a), $z \sim 1$ ULIRGs (Lo Faro et al. 2013), and $z \sim 2$ SMGs (Michałowski et al. 2010). In all galaxy populations shown here, at high $sSFR \gtrsim 10^{-9}$ yr^{-1} the amount of dust compared with stellar content is lower than would be expected from local trends in less extreme galaxies. This is consistent with the results of

Hjorth et al. (2014) who predict the existence of a "maximum attainable dust mass" which causes a turn-over of the relation at high sSFR.

Figure 6 shows another permutation of the three variables $M_{\rm star}$, $M_{\rm dust}$, and SFR, namely the ratio, $M_{\rm dust}/SFR$, plotted against sSFR. It can be seen that there is a strong correlation in the sense that $M_{\rm dust}/SFR$ decreases with increasing sSFR. As in Fig. 5, the three curves correspond to the Karim et al. (2011) MS together with the $M_{\rm dust}$–SFR correlation by da Cunha et al. (2010b). The deviation of this trend with respect to the data at high sSFR is even greater than with the ratio of dust mass to stellar mass and sSFR (see Fig. 5). At high sSFRs, dust mass relative to SFR is much lower than the expected, almost constant, trend. Here, as in previous figures, the GRBHs have properties similar to dusty massive galaxies (e.g., ULIRGs and SMGs) with high sSFRs.

The spread in the dust/stars mass ratios and sSFRs in the GRBHs is due mostly to redshift. In Figs. 5 and 6, the two (IR-detected) galaxies with the highest dust mass relative to their SFR or sSFR are GRB 020819B and 090417B, both relatively local galaxies with $z \sim 0.4$ and $z \sim 0.3$, respectively. These hosts have properties very similar to the $z \sim 0$ galaxies we have included in the comparison. In contrast, the other (IR-detected) GRBHs at similar sSFR are at $z \gtrsim 1$, and have more than 10 times lower $M_{\rm dust}/M_{\rm star}$ and $M_{\rm dust}/SFR$. Indeed, the properties of the GRBHs with $z \gtrsim 1$ lie within the range of ULIRGs and SMGs; more measurements are needed to establish whether a subset of GRBHs truly resemble these IR-luminous galaxies as would be suggested by these results.

There are several possible interpretations of the mutual trends of $M_{\rm dust}$, $M_{\rm star}$, and SFR. $M_{\rm dust}/SFR$ was interpreted by da Cunha et al. (2010b) as a proxy for the dust-to-gas mass ratio of a galaxy because of the gas–SFR scaling relations (Schmidt-Kennicutt, e.g., Kennicutt 1998): $M_{\rm dust}/SFR \propto M_{\rm dust}/M_{\rm gas}$. Thus, the inverse correlation between $M_{\rm dust}/SFR$ and sSFR would imply that dust-to-gas ratios are larger in galaxies with low sSFR because the reservoir of gas available for star formation has been exhausted. A high sSFR would mean that dust-to-gas ratios are lower because of larger gas reservoirs, but the dust content would still be high, given the large $M_{\rm dust}/M_{\rm star}$. On the other hand, Magdis et al. (2012) and Sargent et al. (2013) favor another interpretation, namely that $M_{\rm dust}/SFR$ is inversely proportional (together with a metallicity dependence) to the star-formation efficiency (SFE), defined as the ratio of SFR and gas mass: $M_{\rm dust}/SFR \propto (Z/Z_\odot)\, SFE^{-1} \propto (Z/Z_\odot)\, M_{\rm gas}/SFR$. This is the inverse of the dependence on $M_{\rm gas}$ with respect to that hypothesized by da Cunha et al. (2010b). Magdis et al. (2012) and Sargent et al. (2013) argue that for galaxies on the MS of star formation, SFEs are relatively constant, and lower than for starbursting systems with high sSFR. This would explain the negative correlation between $M_{\rm dust}/SFR$ and sSFR, and its variation with redshift.

We propose a third (related) interpretation based on the idea that in the Rayleigh-Jeans regime, dust mass depends on the monochromatic IR luminosity, L_ν, and inversely on the mean dust temperature, $T_{\rm dust}$. Because SFR is linear with $L_{\rm IR}$ (assuming an optically thick star-formation episode, e.g., Kennicutt 1998), SFR would scale like ${T_{\rm dust}}^{4+\beta}$ since $L_{\rm IR}$ results from integrating L_ν over frequency ν (e.g., Hayward et al. 2011). Thus, $M_{\rm dust}/SFR$ would be inversely proportional to ${T_{\rm dust}}^{5+\beta}$. $T_{\rm dust}$ is expected to vary as some power of the mean radiation field intensity $\langle U \rangle$ ($T_{\rm dust} \propto U^{1/(4+\beta)}$, e.g., Hirashita & Hunt 2004), meaning that $SFR/M_{\rm dust} \propto T_{\rm dust}\, \langle U \rangle$. This would be consistent with the finding by Magdis et al. (2012) that $L_{\rm IR}/M_{\rm dust}$ in $z \sim 2$ IR galaxies increases with $\langle U \rangle$ in the Draine & Li (2007) dust models used to fit their SEDs. Mean $T_{\rm dust}$ would be higher for galaxies with high sSFR, and could be a way to distinguish starbursts from MS galaxies as proposed by Hayward et al. (2012) and Magnelli et al. (2014). Of the objects in our GRBH sample, the two closest hosts, GRB 020819B and GRB 090417B, are apparently MS galaxies, since their properties are consistent with the comparison local galaxy populations. Neither of these objects has any stellar mass produced in a recent burst of star formation (see Fig. 3). On the other hand, the GRBHs at $z \gtrsim 1$ resemble some of the local ULIRGs and $z \sim 2$ SMGs; thus they may be starburst galaxies, at least judging from their position in the right panel of Figs. 5 and 6. Indeed, as suggested by Priddey et al. (2006) and Michałowski et al. (2008, 2010), GRBs may be a way to select warm SMGs, which before *Herschel* were difficult to identify.

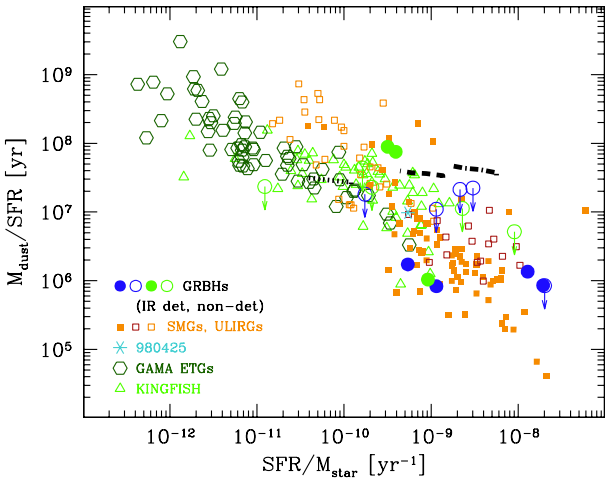

Fig. 6. Ratio of $M_{\rm dust}$/SFR plotted against sSFR. As in Fig. 4, the GRBHs observed by *Herschel* are indicated by filled (for IR detections) and open (IR non-detections) circles, and the other galaxy samples shown are also coded as in Fig. 4. The three curves are the fits of sSFR vs. $M_{\rm star}$ at $z = 0.2 - 0.4$ (dotted left), $z = 1.0 - 1.2$ (dashed middle), and $z = 2.0 - 2.5$ (dot-dashed right) by Karim et al. (2011) as shown in Fig. 4, but here incorporating the dependence of $M_{\rm dust}$ on SFR as found at $z \approx 0$ by da Cunha et al. (2010b) (see also Fig. 5).

5.5. Extinction from SED fitting

Extinction in galaxies is known to correlate both with stellar mass and with SFR (Garn & Best 2010; Garn et al. 2010), although since these latter quantities are related through the star-formation MS, the correlations are probably not independent. We show extinction A_V as estimated by the best-fit GRASIL models plotted against stellar mass in Fig. 7 (left panel) and SFR (right) for the GRBHs and other samples with available data for extinction from SED fitting. The curve in the left panel is the trend found by Garn & Best (2010) for a sample of $z \sim 0$ SDSS galaxies using the Balmer decrement to estimate A_V, and in the right panel, the trend of A_V with SFR found by Garn et al. (2010) for galaxies between $z \sim 0$ and $z \sim 0.8$. Both curves are shown over the ranges in parameters for which they were defined. In Fig. 7, we have converted the empirical A_V curves for Hα to A_V using the extinction curve by Cardelli et al. (1989). Because extinction of emission lines tends to be higher than that of the continuum, we have also applied the recommended correction

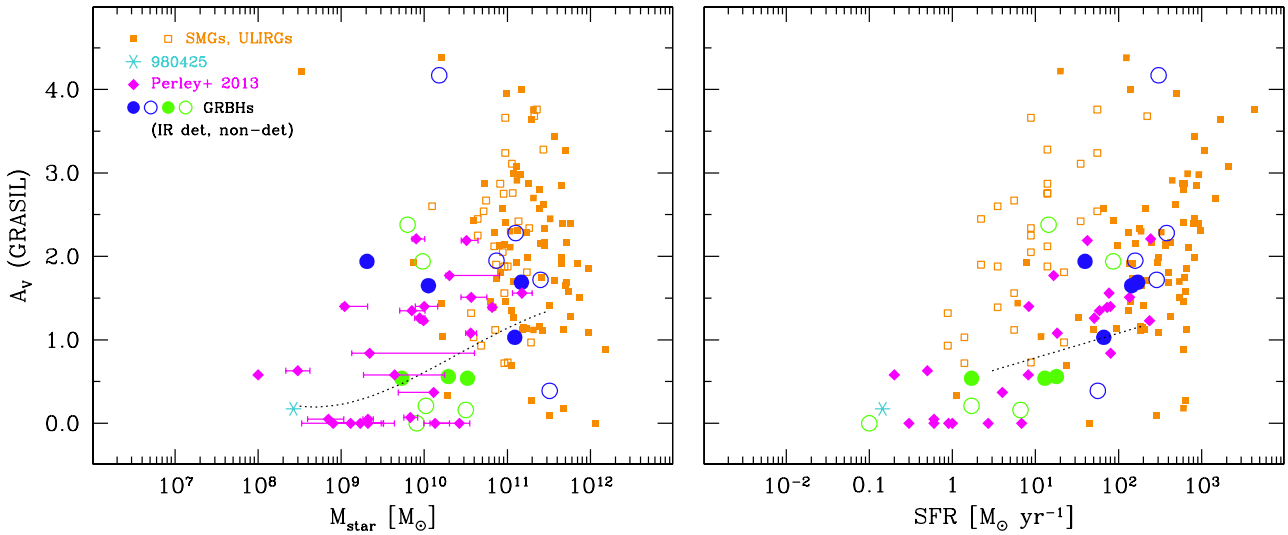

Fig. 7. Extinction A_V (mag) from GRASIL fits (except for those from Perley et al. 2013) plotted against $M_{\rm star}$ (*left panel*) and SFR (*right*). As in Fig. 4, the GRBHs observed by *Herschel* are indicated by filled (for IR detections) and open (IR non-detections) circles, and the other galaxy samples shown are also coded as in Fig. 4. The curves show the trends for galaxies in the Local Universe (*left panel*, Garn & Best 2010), and for $z \sim 0.8$ (*right*, Garn et al. 2010).

factor of 0.44 to both curves (Calzetti et al. 2000; Garn et al. 2010).

Figure 7 shows that for the GRBHs (and the SMGs and ULIRGs), there is a large scatter in A_V for a given $M_{\rm star}$ or SFR, but in general GRASIL A_V's for the GRBHs are consistent with those predicted by both curves. The GRASIL models give an average optical thickness at 0.55 μm, defined as the (natural logarithm) of the ratio of the dust-free flux and the observed flux. We convert this to an optical extinction in magnitudes A_V by multiplying by 1.086. Unlike the GRASIL A_V, the curves shown in Fig. 7 are calculated with the Balmer decrement which implicitly assumes a screen geometry, with a dust screen absorbing the stellar radiation between it and the observer. GRASIL values of A_V, taking into account the dust and stellar spatial distributions, do not differ in a systematic way from the values of A_V inferred by assuming a dust screen (as is usually assumed in optical-near-IR SED fitting).

Perley et al. (2013) compared the A_V in the hosts to the extinction in the GRB afterglow, and found that in most GRBHs the galaxy-wide extinction is consistent to within a factor of 2 to the afterglow A_V. This would imply that the dust is distributed in a fairly homogeneous way, and that local effects are not usually important (although for a counter example see Greiner et al. 2013). The Perley et al. targets were selected on the basis of the afterglow extinction requiring $A_V \gtrsim 1$ mag, making their sample a reasonable representation of dust-obscured GRBs. In terms of dust properties, it should be very similar to our sample which is dominated by the hosts of dark GRBs (14 of 17). Indeed, relative to our GRBHs, there is no noticeable difference in the A_V's of the hosts in Perley et al. (2013), and the GRBHs studied by Perley et al. (2013) appear to follow expected trends of A_V with both $M_{\rm star}$ and SFR. As with other properties studied here, the GRBH population (or at least the dark and/or dusty subset) appears to be normal in terms of dust extinction.

6. GRBHs in context

In the previous sections, we have analyzed the properties of the GRBHs in our sample (and when possible also in Savaglio et al. 2009; Perley et al. 2013), and found that their stellar masses, dust masses, SFR, and dust extinction generally conform to what is known about other star-forming galaxy populations, both locally and up to $z \gtrsim 3$.

Our *Herschel* sample is dominated by hosts of dark GRBs, and the sample studied by Perley et al. (2013) was defined on the basis of high dust extinction ($A_V \gtrsim 1$ mag) in the GRB afterglow. In contrast, the GRBHs analyzed by Savaglio et al. (2009) come almost exclusively from optically bright GRBs. By combining these three samples (e.g., Fig. 4), we have a total of 66 GRB hosts (having eliminated the relatively large overlap among the samples). To our knowledge, this is the largest long-GRBH sample with reliable stellar masses and SFRs compiled to date, with redshifts ranging from $z \sim 0$ to $z \gtrsim 3$ and a median redshift $z_{\rm med} = 1.1$ (see Sect. 2). These 66 GRBHs consist of: 32 hosts of dark GRBs[7] (23 of which are hosts of high-A_V GRB afterglows), and 34 hosts of optically bright GRBs. The resulting fraction of dark GRBs in our combined sample is 48%, slightly higher than the upper limit of the possible fraction of dark bursts ($\lesssim$40%) reported by Greiner et al. (2011). We conclude that our sample comprises a collection of GRBHs that is, if anything, biased towards dark and dusty bursts. Since there has been a dearth of such GRBs in most samples studied up to now, it will provide an ideal test for investigating trends of stellar mass and SFR with redshift.

6.1. GRBH stellar masses as a function of redshift

Here we examine whether GRBs could be unbiased tracers of cosmic co-moving SFR density ρ_* by comparing the stellar masses and sSFRs of our combined GRBH sample with the statistics of star-forming galaxies found in recent large-scale deep multiwavelength surveys. This will be important to establish whether GRBs trace SFR to high redshift in an unbiased way, or whether GRBHs are in some way not representative of typical star-forming galaxy populations.

One of the main arguments against using GRBs to trace ρ_* has been that GRBHs tend to be less massive than representative

[7] As mentioned in Sect. 2, we define a dark GRB as one with optical-to-X-ray spectral index $\beta_{\rm ox} < 0.5$.

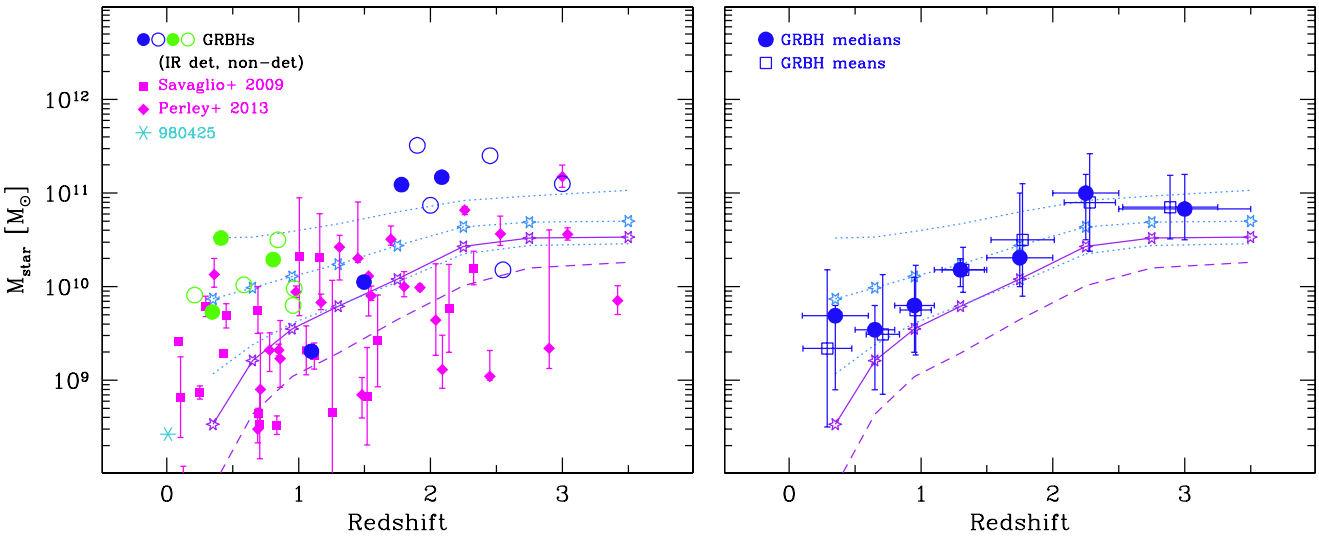

Fig. 8. Stellar mass M_{star} plotted against redshift. Individual GRBHs are shown in the *left panel*, and medians and means in the *right panel*. The GRBHs shown in the *left panel* and observed by *Herschel* are indicated by filled (for IR detections) and open (IR non-detections) circles, and the other GRBH samples are coded as in Fig. 4. The curves show the medians of the star-forming population as a function of z (see text). The solid line connecting open (purple) stars gives the median M_{star} as a function of z, and the dotted line connecting the open (light blue) stars corresponds to the SFR-weighted medians of M_{star} as described in the text; the dotted lines below and above these weighted medians show the upper and lower quartiles, respectively. The lowest dashed (purple) line indicates the mass limits of the survey. In *the right panel*, the GRBH medians shown as filled circles are calculated in the same redshift bins as the UltraVISTA comparison (Ilbert et al. 2013). The vertical error bars correspond to the upper and lower quartiles of the GRBH distributions, and the horizontal error bars to the width of the redshift bins. The open squares give the GRBH means within each redshift bin, and the error bars the standard deviation. For the GRBH statistics, we considered only the hosts with M_{star} above the Ilbert et al. (2013) survey lower-mass limit M_{low}.

galaxy populations. Especially at $z \lesssim 1.5$, the host population has been previously found to favor low stellar masses, and when nebular metallicities can be measured, also low metal abundance (Savaglio et al. 2009; Levesque et al. 2010a). Now, with more data available for hosts of dark and dust-extinguished GRBs, we can reassess the question of stellar masses and SFRs in GRBHs.

Our approach is to compare the distributions in redshift of M_{star} and sSFR of our GRBH sample with the statistics of 220 000 galaxies selected from the deep ($K_s < 24$ AB mag) wide UltraVISTA survey (McCracken et al. 2012; Ilbert et al. 2013). The unprecedented depth and coverage of this survey obviates the need to compensate for cosmic variance, and enables a robust comparison with the GRBH population. We make no corrections to the statistics of the GRBH sample, implicitly assuming that all possible hosts have been identified, that their redshifts have been determined, and that all GRBs that have exploded have been localized, and their host detected. Clearly none of these assumptions are correct (e.g., Fynbo et al. 2009; Krühler et al. 2012; Salvaterra et al. 2012; Hjorth et al. 2012), but there is no straightforward method for adjusting any of the statistics of our compiled GRBH sample.

As a comparison quantitative benchmark of stellar mass as a function of redshift, we have adopted the double Schechter (Schechter 1976) functions given by Ilbert et al. (2013) for the star-forming galaxies in the UltraVISTA survey; these fits are based on ~135 000 star-forming galaxies selected with a two-color criterion (restframe NUV$-r^+$, r^+-J) to separate them from quiescent galaxies. At all redshifts, star-forming galaxies are $\gtrsim$6 times more common in number than quiescent ones, and at redshifts $z \lesssim 1.5$, they tend to be a factor of ~2 less massive. At each redshift, to calculate the median stellar mass we have integrated the double Schechter functions of Ilbert et al. (2013) from the lower mass limit dictated by the depth of their survey M_{low} to 10^{13} $M_\odot$. Because we want to test the hypothesis that GRBs are tracing star formation, the stellar mass integrands have been weighted by SFR as determined from the analytical functions of SFR as a function of redshift by Karim et al. (2011). Once we have the integrals as a function of z, it is straightforward (either numerically or analytically) to calculate the median stellar mass, the median stellar mass weighted by SFR, and their 25th and 75th percentile dispersions.

Figure 8 shows the results of these calculations graphically; the left panel shows the individual GRBHs, and the medians and means of the host distribution are shown on the right. Table 3 reports the statistics of the combined GRBH sample shown in the figure; the GRBH medians, means, and dispersions are calculated without considering the hosts with M_{star} below M_{low} of the survey (see Col. 2 of Table 3). The curves in both panels of Fig. 8 correspond to median M_{star} (solid line) and the median SFR-weighted M_{star} (dotted line) of the UltraVISTA survey, as inferred from integrating the double Schechter functions given by Ilbert et al. (2013). The medians of SFR-weighted M_{star} fall above the non-weighted medians because more massive galaxies have higher SFR, thus skewing the median masses to higher values (e.g., Karim et al. 2011). The left panel of Fig. 8 shows clearly that beyond $z \sim 0.5$, GRBs can identify galaxies of such low mass that they fall well below the limits of even the deep UltraVISTA survey (as shown by the dashed line).

At all redshifts, the GRBH median stellar masses fall close to or slightly below the expected median of the SFR-weighted star-forming galaxies at those redshifts. One possible exception is the $z \sim 2$ bin, where the GRBH median and mean M_{star} both lie *above* the SFR-weighted median of the UltraVISTA distribution. Taking the results at face value, and within the mass limits of UltraVISTA, the distributions (medians and dispersions) of the GRBH M_{star} all fall within the range of 50% of the UltraVISTA distribution of normal star-forming galaxies. Thus we would conclude that there is no strong evidence that the host population

Table 3. Combined GRBH $M_{\rm star}$, sSFR vs. redshift statistics.

Central z	Total number[a]	log $M_{\rm low}$[b]	Number $M_{\rm star} \geq M_{\rm low}$	log($M_{\rm star}$) median ($M_\odot$)	25th% ($M_\odot$)	75th% ($M_\odot$)	log($sSFR$) median ($\rm yr^{-1}$)	25th% ($\rm yr^{-1}$)	75th% ($\rm yr^{-1}$)
(1)	(2)	(3)	(4)	(5)	(6)	(7)	(8)	(9)	(10)
0.35	11	7.86	11	9.69	8.9	9.8	−9.29	−8.8	−9.5
0.65	8	8.64	6	9.54	8.9	9.8	−9.11	−8.8	−9.3
0.95	10	9.04	9	9.80	9.3	10.1	−8.88	−8.5	−9.3
1.30	8	9.29	6	10.18	10.0	10.3	−9.08	−7.9	−9.9
1.75	10	9.65	8	10.31	10.0	11.0	−8.98	−8.3	−9.3
2.25	8	10.01	4	11.00	10.5	11.2	−8.95	−8.8	−9.1
3.00	7	10.24	4	10.83	10.6	11.2	−8.90	−8.4	−9.3

Notes. [(a)] These numbers do not add up to the total of 66 GRBHs in our combined sample because three have $z \leq 0.1$ (GRB 060505, GRB 060218, GRB 980425) and have not been included in the statistics. [(b)] These are the lower limits in the stellar masses of the survey by Ilbert et al. (2013). Column (1): Central redshift of the bin; Col. 2: total number of GRBHs within the redshift bin; Col. (3): the lower mass limit $M_{\rm low}$ of the UltraVISTA survey at this redshift (Ilbert et al. 2013); Col. (4): total number of GRBHs in this bin with $M_{\rm star} \geq M_{\rm low}$; Cols. (5–7): median and percentiles of the GRBH $M_{\rm star}$ within this redshift bin; Cols. (8–10): median and percentiles of the GRBH sSFR within this redshift bin.

is not representative of typical star-forming galaxies; on the contrary GRBHs are apparently similar to the more general star-forming galaxy population at least for $z \lesssim 3$.

This result contrasts with Perley et al. (2013) who found that at $z \lesssim 1.5$, there is a "highly significant aversion" to massive GRBHs, namely a preference for low-mass systems that exceeds expectations for a purely SFR-selected sample. The most likely reason for the difference between our conclusions and theirs is the different comparison samples and the comparison methodology. Perley et al. (2013) use the narrow but deep survey ($K_{\rm s} < 23$ Vega mag, 24.8 AB mag) by Kajisawa et al. (2009, MOIRCS Deep Survey, MODS), slightly deeper than the UltraVISTA survey but with ∼25 times fewer galaxies in the $z = 0.5-1.0$ redshift bins because of the narrow field-of-view. Although the depth of the two surveys is comparable, the statistical accuracy is much greater with UltraVISTA. Moreover, the MODS survey does not distinguish between quiescent and star-forming galaxies, making it impossible to compare GRBHs with only the star-forming population. As mentioned above, at redshifts $z \lesssim 1.5$ star-forming galaxies tend to be less massive by a factor of 2 or more than quiescent populations. Our results show that the GRBHs are as massive or even more massive than the (non-SFR-weighted) star-forming galaxy populations at all redshifts; this is a robust result (see Fig. 8) and shows the importance of weighting $M_{\rm star}$ with SFR. Another possible reason for the contrast is that many of the least massive hosts fall below the mass limits of the UltraVISTA survey (and the MODS survey Kajisawa et al. 2009), and we thus did not consider them in the GRBH statistics. Although Perley et al. (2013) checked this and concluded that completeness was not a problem for the MODS comparison, combined with other factors this could also contribute to the difference between our conclusions. A final possible reason is the double-episode SFH incorporated by our GRASIL fitting, as opposed to the single star-formation episode used by Perley et al. (2013); as mentioned in Sect. 5.1, this is known to give larger stellar masses (Michałowski et al. 2012a).

We do find, however, a possible trend of host masses being less massive then the UltraVISTA SFR-weighted $M_{\rm star}$ median up to $z \lesssim 1$, but the dispersions are large. Besides Perley et al. (2013), many previous studies (e.g., Le Floc'h et al. 2003; Fynbo et al. 2003; Boissier et al. 2013) also found that GRBHs are a biased representation of star-forming galaxies because they tend to be less massive and more metal-poor for $z \lesssim 1.5$ (although see Michałowski et al. 2012b). However, such conclusions are probably sample-dependent. We find that the host masses as a function of redshift depend on the percentage of dark or dusty bursts within a given redshift bin. At all redshifts, the hosts of dark bursts are more massive than the median GRBH $M_{\rm star}$ at that redshift[8].

Even though our sample is relatively large, the numbers are still sparse when distributed in redshift space. Indeed, the largest discrepancy relative to the star-forming weighted median $M_{\rm star}$ is the $z = 0.65$ bin; it contains only two hosts of dark GRBs which are also the most massive in that bin. Because of the small number (4) hosts of non-dark GRBs in the same redshift bin, one more dark GRB host at a similar mass ($\sim 10^{10}\,M_\odot$) could have raised the median to ∼dex(9.8) $M_\odot$ (the same median mass as the $z = 0.95$ bin),

6.2. SFR and sSFR of GRBHs as a function of redshift

We now examine trends of sSFR with redshift for our sample and compare them with the properties of the COSMOS sample analyzed by Karim et al. (2011). Figure 9 shows sSFR of the GRBHs and $z \sim 1-2$ ULIRGs and SMGs in the left panel plotted against redshift, and in the right panel the GRBH medians and mean sSFR. The curves in both figures correspond to the trends of sSFR with z for three specific values of $M_{\rm star}$ (dex(9.6) $M_\odot$, dex(10.4) $M_\odot$, >dex(11) $M_\odot$) as found by Karim et al. (2011). Because the strongest trend of sSFR is with redshift rather than with $M_{\rm star}$ (e.g., Karim et al. 2011), to calculate the medians for the GRBHs we have binned only in redshift, rather than again sub-dividing into mass bins; this helps conserve statistical significance given our relatively small sample size. To be consistent with the $M_{\rm star}$ statistics, we considered only the hosts with $M_{\rm star}$ larger than the UltraVISTA lower-mass limit. Columns 8–10 of Table 3 give the median sSFR as a function of z for our host sample.

For $z \lesssim 1$, the median sSFRs of the hosts are always higher than the curves given by Karim et al. (2011). This tendency to high sSFRs is almost certainly related to the tendency toward lower $M_{\rm star}$ seen in Fig. 8. Beyond $z \sim 1$, the median GRBH sSFR is similar to that expected values for massive galaxies, again consistently with the trends for $M_{\rm star}$ shown in Fig. 8. We conclude that at low redshift, $z \lesssim 1$, GRBHs tend to have slightly

[8] The host of GRB 070306 is an exception to this, having $M_{\rm star}$ roughly equal to the median of the distribution.

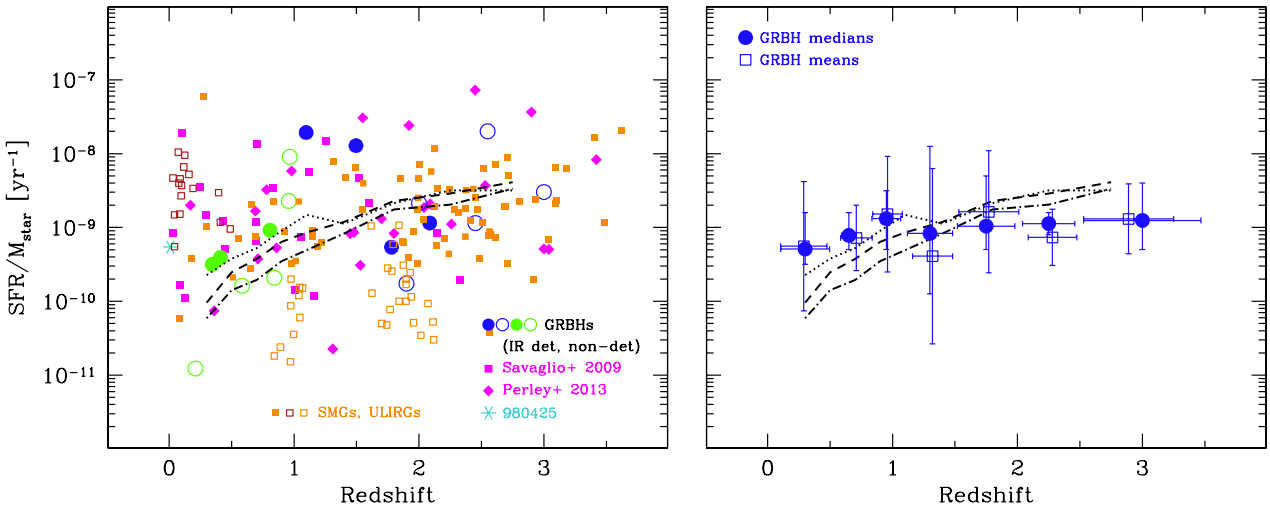

Fig. 9. sSFR (=SFR/M_{star}) plotted against redshift. Individual GRBHs, SMGs, and ULIRGs are shown in the *left panel*, and medians and means of the GRBH sample in the *right*. As in Fig. 4, in the *left panel* the GRBHs observed by *Herschel* are indicated by filled (for IR detections) and open (IR non-detections) circles, and the other GRBH samples shown are also coded as in Fig. 4. The curves show the results from Karim et al. (2011), and correspond to three values of log (M_{star}) = 9.6 (dotted line), 10.4 (dashed), and >11 $M_{\odot}$ (dot-dashed). The GRBH medians in the *right panel*, shown as filled circles for the lowest-mass bins at a given redshift, and and filled squares for the highest-mass bins as described in the text. The vertical error bars correspond to the upper and lower quartiles of the GRBH distributions, and the horizontal error bars to the width of the redshift bins (for the GRBH data). Open squares show the means of the GRBH distributions within each redshift bin, and the error bars correspond to the standard deviation. As in Fig. 8, for the GRBH statistics, we considered only the hosts with M_{star} above the Ilbert et al. (2013) survey M_{low} limit.

lower M_{star}, and slightly higher sSFRs than the star-forming galaxy populations at those redshifts. However, the difference is dominated by large scatter, and disappears entirely beyond $z \gtrsim 1$.

6.3. Reconciling our results

In this paper, we have focused on dust mass, stellar mass and sSFRs, and have concluded that, although there is large dispersion, the GRBH population appears to have similar characteristics as the more general star-forming galaxy population for $z \lesssim 3$. However, there are numerous studies based on other aspects of GRBs and their host galaxies that reach a different conclusion. Here we attempt to summarize these and formulate a view consistent with all the evidence.

The supposed inability of GRBHs to trace cosmic SFR is most pronounced at low redshift, $z \lesssim 1$. In this redshift range, the GRB property that has been most under scrutiny is metallicity, namely the finding that $z \lesssim 1$ GRBHs are more metal poor than general star-forming galaxy populations (e.g., Savaglio et al. 2009; Han et al. 2010; Levesque et al. 2010a). For a given M_{star}, metallicities of nearby GRBHs are found to fall below the SFR-weighted mass-metallicity relation (Kocevski & West 2011; Graham & Fruchter 2013). On the other hand, Mannucci et al. (2011) find that GRBHs differ from the mass-metallicity relation because of their high SFRs, not because their O/H is anomalously low for their M_{star}. Indeed, many GRBHs have high sSFR, and would be considered starbursts since they lie well above the MS of star-formation (see e.g., Fig. 4). Because of the so-called Fundamental Metallicity Relation or Fundamental Plane of M_{star}, O/H, and SFR (e.g., Mannucci et al. 2010; Hunt et al. 2012), at a given M_{star}, GRBHs are thus expected to be more metal poor than galaxies along the MS. The relatively low abundances and high sSFRs of GRBHs essentially trace a "starburst sequence" of the mass–metallicity relation as shown by Mannucci et al. (2011).

In any case, if there is any metallicity bias at $z \lesssim 1$, it appears to set in at relatively high metallicities ($Z \lesssim 50\%\ Z_{\odot}$, Hao & Yuan 2013; Graham & Fruchter 2013), and is quantitatively small (Wolf & Podsiadlowski 2007). There is possibly some evidence that such a bias could change with redshift up to $z \lesssim 1$ (Boissier et al. 2013). Theoretical models show only a moderate preference for low metallicity (Trenti et al. 2013), although even this could arise from a bias because of using only redshifts measured from optical afterglows (Wanderman & Piran 2010).

In fact, most of the above studies were based on relatively small samples of GRBHs with clearly detected optical afterglows (e.g., Han et al. 2010; Kocevski & West 2011; Graham & Fruchter 2013). The problem with analyzing metallicity in galaxies at $z \lesssim 1$ is that optical spectra are needed, which requires afterglows or host galaxies that are sufficiently bright to observe spectroscopically. Hence, such analyses tend to exclude, by design and by necessity, dark hosts, thus possibly compromising the general applicability of the conclusions about trends with metallicity.

Another aspect of $z \lesssim 1$ GRBs that could indicate that they are not unbiased tracers of star formation is their environments and the kinds of galaxies that they reside in. The environments of nearby long GRBs have been found to differ from those of core-collapse supernovae (CCSNe), leading to the conclusion that GRBs are associated with only the most massive stars and tend to reside in fainter and more irregular galaxies than the hosts of CCSNe (Fruchter et al. 2006). However, this result is not confirmed by Kelly et al. (2008) and Leloudas et al. (2010) who found that type Ic SNe, those associated with long GRBs, are more likely to erupt in the brightest regions of their hosts, similarly to GRBs themselves. Nevertheless, the relations of stellar mass with galaxy morphology, SFR, and metallicity make it difficult to establish whether low-redshift GRBs tend to occur in low-mass galaxies because they are metal poor or because such galaxies dominate star-forming populations at these redshifts. Given that GRBs select galaxies with a SFR weighting scheme, the predominance of metal-poor low-mass galaxies at $z \lesssim 1$ could simply be a consequence of the high fractions of low-mass ($M_{star} \leq 10^{10}\ M_{\odot}$), blue, high sSFR ("high activity") systems which are known to dominate the star-forming galaxy population for $0.5 \lesssim z \lesssim 1$ (Ilbert et al. 2010).

At redshifts $z \gtrsim 1$, the main evidence pointing toward a potential inability of GRBH to trace cosmic SFR density, ρ_*, is based on observed cumulative redshift distributions. In contrast to the smooth decline in ρ_* for $z \gtrsim 3$ inferred from UV continuum surveys (e.g., Hopkins & Beacom 2006; Bouwens et al. 2011; Ellis et al. 2013), GRB rates need ρ_* to remain flat to $z \gtrsim 8$ (e.g., Kistler et al. 2009; Butler et al. 2010; Robertson & Ellis 2012; Jakobsson et al. 2012). This could be because the bulk of star formation at high redshifts occurs in galaxies that are below the detection limit of even the deepest UV surveys (e.g., Tanvir et al. 2012; Trenti et al. 2012, 2013); such a faint population would play an important role in cosmic reionization (Finkelstein et al. 2012). Moreover, when a series of biases are taken into account when comparing the rate of GRBs and ρ_*, there is apparently no discrepancy between the normal star-forming galaxy population and the hosts traced by GRBs (Elliott et al. 2012). This debate is far from being resolved, but wider and deeper galaxy surveys together with further analysis of unbiased GRB samples will provide more constraints.

Finally, there is the ISM content of GRBHs which in part we have examined in this paper through *Herschel* observations. Because star formation is associated with molecular gas, and because of the high sSFRs in GRBHs, GRB host galaxies would be expected to have a fairly robust molecular hydrogen H_2 content. However, tracing H_2 through GRB absorption-line or damped Lyα systems (DLAs) has been quite difficult. Molecular gas at $z \gtrsim 2$ has been detected so far in only two and possibly a third GRB-DLA (Prochaska et al. 2009; Fynbo et al. 2006; Krühler et al. 2013). One of these (GRB 080607) is metal-rich, and one is metal-poor (GRB 120815A), so there is no clear trend even with these small numbers. Because sightlines with low dust depletion (and low metallicity) favor the detection of DLAs, selection effects have significant impact on the study of H_2 in GRB-DLAs (Krühler et al. 2013). Larger samples of afterglows observed with powerful instruments such as the VLT/X-Shooter and ALMA will undoubtedly help better understand the molecular content in GRBHs.

7. Summary and conclusions

For the first time, we are able to place constraints on dust emission in a significant sample of the hosts of long GRBs. We have observed with *Herschel* 17 GRBHs from $z \sim 0.2$ to $z \sim 3$, and detected dust emission in 7. The probability of IR detection in the dark subset of our sample is 43%, compared to $\lesssim$20% from previous attempts to detect IR emission which targeted hosts of optically bright GRBs (e.g., Tanvir et al. 2004; Le Floc'h et al. 2006). Fitting the multiwavelength SEDs with GRASIL gives dust and stellar masses, SFRs, and dust extinction, and enables a comparison of these properties in GRBHs with other star-forming galaxy populations at similar redshift. This comparison shows that GRBHs at $z \gtrsim 0.5$ tend to be galaxies with high sSFRs and high dust-to-stellar mass ratios, but are in any case similar in terms of $M_{\rm star}$, SFR, and A_V to other populations. The $M_{\rm dust}/M_{\rm star}$ ratios and sSFR of GRBHs are similar to SMGs and ULIRGs at similar redshifts. The trends of $M_{\rm dust}/SFR$ suggest that GRBs may select warm SMG-like objects, which before *Herschel* were difficult to identify.

To investigate whether GRBs can be used to trace co-moving SFR in the universe, we have incorporated additional GRBHs in our analysis and compared them with trends of redshift for $M_{\rm star}$ and sSFR as given by the recent UltraVISTA survey of 220 000 galaxies (~135 000 star-forming). The results show that the stellar masses of GRBHs in our combined sample lie within the range of 50% of the UltraVISTA star-forming galaxy population from $z \sim 0.3$ to $z \sim 3$, although there is a large dispersion. The sSFRs of the GRBHs tend to be high, but are also within the range of values expected for star-forming galaxies at similar redshifts. Thus we conclude that GRBs select galaxies that are representative of the more general population; hence they should trace the cosmic SFRD in an unbiased way.

Our sample is dominated by hosts of dark GRBs, and dark hosts have $M_{\rm star}$ above the GRBH median in all redshift bins. Because dark and dusty bursts tend to be found in more mature, metal-rich galaxies, it is possible that this sample composition is driving our conclusion that GRBH are unbiased tracers of star formation. Better statistics are needed, together with careful SED fitting, to better address the properties of the hosts of dark GRBs, their impact on the GRBH population as a whole, and whether the hosts of GRBs are generally representative of high-z galaxies.

Acknowledgements. We warmly thank Ruben Salvaterra for enlightening discussions, and Iván Oteo for giving us the data for the LBG $z = 1, 2$ samples. We are grateful to the anonymous referee for insightful and timely comments that improved the clarity of the manuscript. MJM and is a postdoctoral researcher of the FWO-Vlaanderen (Belgium), and acknowledges support from the Science and Technology Facilities Council. A.R. acknowledges support from the Thüringer Landessternwarte Tautenburg, and S.B., V.D.E., L.K.H., E.P., and A.R. are grateful for support from PRIN-INAF 2012/13. S.S. acknowledges support from the Bundesministerium für Wirtschaft and Technologie through DLR (Deutsches Zentrum für Luft- und Raumfahrt e.V.) FKZ 50 OR 1211; and P.S. acknowledges support through the Sofja Kovalevskaja Award from the Alexander von Humboldt Foundation of Germany. Part of the funding for GROND (both hardware as well as personnel) was generously granted from the Leibniz-Prize to Prof. G. Hasinger (DFG grant HA 1850/28-1). Use was made of the NASA/IPAC Extragalactic Database (NED), and the public website for GRB host galaxy data (`http://www.grbhosts.org/`) maintained by S. Savaglio and collaborators.

References

Aoki K., Tanaka, I., Kawai N., et al. 2006, GCN Circular N. 5522
Aoki K., Tanaka, I., Nakata, F. et al. 2009, GCN Circular N. 9145
Barnard, V. E., Blain, A. W., Tanvir, N. R., et al. 2003, MNRAS, 338, 1
Berger, E., Kulkarni, S. R., & Frail, D. A. 2001, ApJ, 560, 652
Berger, E., Cowie, L. L., Kulkarni, S. R., et al. 2003, ApJ, 588, 99
Berger, E., Fox, D. B., Kulkarni, S. R., Frail, D. A., & Djorgovski, S. G. 2007, ApJ, 660, 504
Bianchi, S. 2013, A&A, 552, A89
Bloom, J. S., Kulkarni, S. R., & Djorgovski, S. G. 2002, AJ, 123, 1111
Boissier, S., Buat, V., & Ilbert, O. 2010, A&A, 522, A18
Boissier, S., Salvaterra, R., Le Floc'h, E., et al. 2013, A&A, 557, A34
Bouwens, R. J., Illingworth, G. D., Labbe, I., et al. 2011, Nature, 469, 504
Buat, V., Giovannoli, E., Burgarella, D., et al. 2010, MNRAS, 409, L1
Butler, N. R., Bloom, J. S., & Poznanski, D. 2010, ApJ, 711, 495
Calzetti, D., Armus, L., Bohlin, R. C., et al. 2000, ApJ, 533, 682
Campisi, M. A., De Lucia, G., Li, L.-X., Mao, S., & Kang, X. 2009, MNRAS, 400, 1613
Campisi, M. A., Tapparello, C., Salvaterra, R., Mannucci, F., & Colpi, M. 2011, MNRAS, 417, 1013
Cardelli, J. A., Clayton, G. C., & Mathis, J. S. 1989, ApJ, 345, 245
Castro Cerón, J. M., Michałowski, M. J., Hjorth, J., et al. 2010, ApJ, 721, 1919
Castro-Tirado, A. J., Bremer, M., McBreen, S., et al. 2007, A&A, 475, 101
Chabrier, G. 2003, PASP, 115, 763
Chapman, S. C., Smail, I., Windhorst, R., Muxlow, T., & Ivison, R. J. 2004, ApJ, 611, 732
Chary, R., Berger, E., & Cowie, L. 2007, ApJ, 671, 272
Chen, H.-W., Perley, D. A., Wilson, C. D., et al. 2010, ApJ, 723, L218
Christensen, L., Hjorth, J., & Gorosabel, J. 2004, A&A, 425, 913
Covino, S., Melandri, A., Salvaterra, R., et al. 2013, MNRAS, 432, 1231
Cucchiara, A., Levan, A. J., Fox, D. B., et al. 2011, ApJ, 736, 7
da Cunha, E., Charmandaris, V., Díaz-Santos, T., et al. 2010a, A&A, 523, A78
da Cunha, E., Eminian, C., Charlot, S., & Blaizot, J. 2010b, MNRAS, 403, 1894
D'Elia, V. 2013, EAS Pub. Ser., 61, 247
de Ugarte Postigo, A., Lundgren, A., Martín, S., et al. 2012, A&A, 538, A44
Djorgovski, S. G., Kulkarni, S. R., Bloom, J. S., et al. 1998, ApJ, 508, L17
Djorgovski, S. G., Frail, D. A., Kulkarni, S. R., et al. 2001, ApJ, 562, 654
Djorgovski, S. G., Bloom, J. S., & Kulkarni, S. R. 2003, ApJ, 591, L13

Draine, B. T., & Li, A. 2007, ApJ, 657, 810
Elbaz, D., Dickinson, M., Hwang, H. S., et al. 2011, A&A, 533, A119
Elliott, J., Greiner, J., Khochfar, S., et al. 2012, A&A, 539, A113
Elliott, J., Krühler, T., Greiner, J., et al. 2013, A&A, 556, A23
Ellis, R. S., McLure, R. J., Dunlop, J. S., et al. 2013, ApJ, 763, L7
Fazio, G. G., Hora, J. L., Allen, L. E., et al. 2004, ApJS, 154, 10
Finkelstein, S. L., Papovich, C., Ryan, R. E., et al. 2012, ApJ, 758, 93
Fruchter, A. S., Levan, A. J., Strolger, L., et al. 2006, Nature, 441, 463
Fynbo, J. P. U., Jakobsson, P., Möller, P., et al. 2003, A&A, 406, L63
Fynbo, J. P. U., Starling, R. L. C., Ledoux, C., et al. 2006, A&A, 451, L47
Fynbo, J. P. U., Jakobsson, P., Prochaska, J. X., et al. 2009, ApJS, 185, 526
Garn, T., & Best, P. N. 2010, MNRAS, 409, 421
Garn, T., Sobral, D., Best, P. N., et al. 2010, MNRAS, 402, 2017
Gorosabel, J., Klose, S., Christensen, L., et al. 2003, A&A, 409, 123
Graham, J. F., & Fruchter, A. S. 2013, ApJ, 774, 119
Greiner, J., Bornemann, W., Clemens, C., et al. 2008, PASP, 120, 405
Greiner, J., Krühler, T., Klose, S., et al. 2011, A&A, 526, A30
Greiner, J., Krühler, T., Nardini, M., et al. 2013, A&A, 560, A70
Greve, T. R., Bertoldi, F., Smail, I., et al. 2005, MNRAS, 359, 1165
Griffin, M. J., Abergel, A., Abreu, A., et al. 2010, A&A, 518, L3
Hao, J.-M., & Yuan, Y.-F. 2013, ApJ, 772, 42
Han, X. H., Hammer, F., Liang, Y. C., et al. 2010, A&A, 514, A24
Hashimoto, T., Ohta, K., Aoki, K., et al. 2010, ApJ, 719, 378
Hatsukade, B., Kohno, K., Endo, A., Nakanishi, K., & Ohta, K. 2011, ApJ, 738, 33
Hatsukade, B., Hashimoto, T., Ohta, K., et al. 2012, ApJ, 748, 108
Hayward, C. C., Kereš, D., Jonsson, P., et al. 2011, ApJ, 743, 159
Hayward, C. C., Jonsson, P., Kereš, D., et al. 2012, MNRAS, 424, 951
Hirashita, H., & Hunt, L. K. 2004, A&A, 421, 555
Hjorth, J., Malesani, D., Jakobsson, P., et al. 2012, ApJ, 756, 187
Hjorth, J., Gall, C., & Michałowski, M. J. 2014, ApJ, 782, L23
Holland, S., Andersen, M., Hjorth, J., et al. 2000, GCN Circular, 753
Holland, S. T., Sbarufatti, B., Shen, R., et al. 2010, ApJ, 717, 223
Hopkins, A. M., & Beacom, J. F. 2006, ApJ, 651, 142
Hunt, L., Palazzi, E., Rossi, A., et al. 2011, ApJ, 736, L36
Hunt, L., Magrini, L., Galli, D., et al. 2012, MNRAS, 427, 906
Iglesias-Páramo, J., Buat, V., Hernández-Fernández, J., et al. 2007, ApJ, 670, 279
Ilbert, O., Salvato, M., Le Floc'h, E., et al. 2010, ApJ, 709, 644
Ilbert, O., McCracken, H. J., Le Fèvre, O., et al. 2013, A&A, 556, A55
Jakobsson, P., Hjorth, J., Fynbo, J. P. U., et al. 2004, ApJ, 617, L21
Jakobsson, P., Frail, D. A., Fox, D. B., et al. 2005, ApJ, 629, 45
Jakobsson, P., Hjorth, J., Malesani, D., et al. 2012, ApJ, 752, 62
Jaunsen, A. O., Rol, E., Watson, D. J., et al. 2008, ApJ, 681, 453
Kajisawa, M., Ichikawa, T., Tanaka, I., et al. 2009, ApJ, 702, 1393
Kann, D. A., Klose, S., Zhang, B., et al. 2010, ApJ, 720, 1513
Karim, A., Schinnerer, E., Martínez-Sansigre, A., et al. 2011, ApJ, 730, 61
Kelly, P. L., Kirshner, R. P., & Pahre, M. 2008, ApJ, 687, 1201
Kennicutt, R. C., Jr. 1998, ARA&A, 36, 189
Kennicutt, R. C., Calzetti, D., Aniano, G., et al. 2011, PASP, 123, 1347
Kistler, M. D., Yüksel, H., Beacom, J. F., Hopkins, A. M., & Wyithe, J. S. B. 2009, ApJ, 705, L104
Kocevski, D., & West, A. A. 2011, ApJ, 735, L8
Krühler, T., Küpcü Yoldaş, A., Greiner, J., et al. 2008, ApJ, 685, 376
Krühler, T., Greiner, J., Schady, P., et al. 2011, A&A, 534, A108
Krühler, T., Malesani, D., Milvang-Jensen, B., et al. 2012, ApJ, 758, 46
Krühler, T., Ledoux, C., Fynbo, J. P. U., et al. 2013, A&A, 557, A18
Küpcü Yoldaş, A., Greiner, J., Klose, S., Krühler, T., & Savaglio, S. 2010, A&A, 515, L2
Le Borgne, D., & Rocca-Volmerange, B. 2002, A&A, 386, 446
Le Floc'h, E., Duc, P.-A., Mirabel, I. F., et al. 2002, ApJ, 581, L81
Le Floc'h, E., Duc, P.-A., Mirabel, I. F., et al. 2003, A&A, 400, 499
Le Floc'h, E., Charmandaris, V., Forrest, W. J., et al. 2006, ApJ, 642, 636
Le Floc'h, E., Charmandaris, V., Gordon, K., et al. 2012, ApJ, 746, 7
Leloudas, G., Sollerman, J., Levan, A. J., et al. 2010, A&A, 518, A29
Levan, A., Fruchter, A., Rhoads, J., et al. 2006, ApJ, 647, 471
Levesque, E. M., Kewley, L. J., Berger, E., & Zahid, H. J. 2010a, AJ, 140, 1557
Levesque, E. M., Kewley, L. J., Graham, J. F., & Fruchter, A. S. 2010b, ApJ, 712, L26
Lo Faro, B., Franceschini, A., Vaccari, M., et al. 2013, ApJ, 762, 108
MacFadyen, A. I., & Woosley, S. E. 1999, ApJ, 524, 262
Magdis, G. E., Daddi, E., Béthermin, M., et al. 2012, ApJ, 760, 6
Magnelli, B., Lutz, D., Saintonge, A., et al. 2014, A&A, 561, A86
Maiolino, R., Nagao, T., Grazian, A., et al. 2008, A&A, 488, 463
Makovoz, D., & Marleau, F. R. 2005, PASP, 117, 1113
Mannucci, F., Cresci, G., Maiolino, R., et al. 2009, MNRAS, 398, 1915
Mannucci, F., Cresci, G., Maiolino, R., Marconi, A., & Gnerucci, A. 2010, MNRAS, 408, 2115
Mannucci, F., Salvaterra, R., & Campisi, M. A. 2011, MNRAS, 414, 1263
McCracken, H. J., Milvang-Jensen, B., Dunlop, J., et al. 2012, A&A, 544, A156
Melandri, A., Sbarufatti, B., D'Avanzo, P., et al. 2012, MNRAS, 421, 1265
Michałowski, M. J., Hjorth, J., Castro Cerón, J. M., & Watson, D. 2008, ApJ, 672, 817
Michałowski, M. J., Hjorth, J., Malesani, D., et al. 2009, ApJ, 693, 347
Michałowski, M., Hjorth, J., & Watson, D. 2010, A&A, 514, A67
Michałowski, M. J., Dunlop, J. S., Cirasuolo, M., et al. 2012a, A&A, 541, A85
Michałowski, M. J., Kamble, A., Hjorth, J., et al. 2012b, ApJ, 755, 85
Michałowski, M. J., Hunt, L. K., Palazzi, E., et al. 2014, A&A, 562, A70
Molinari, S., Schisano, E., Faustini, F., et al. 2011, A&A, 530, A133
Nguyen, H. T., Schulz, B., Levenson, L., et al. 2010, A&A, 518, L5
Niino, Y., Choi, J.-H., Kobayashi, M. A. R., et al. 2011, ApJ, 726, 88
Noeske, K. G., Weiner, B. J., Faber, S. M., et al. 2007, ApJ, 660, L43
Oteo, I., Bongiovanni, Á., Magdis, G., et al. 2013a, MNRAS, 439, 1337
Oteo, I., Magdis, G., Bongiovanni, Á., et al. 2013b, MNRAS, 435, 158
Ott, S. 2010, ASP Conf. Ser., 434, 139
Paczynski, B. 1998, ApJ, 494, L45
Pellizza, L. J., Duc, P.-A., Le Floc'h, E., et al. 2006, A&A, 459, L5
Perley, D. A., & Perley, R. A. 2013, ApJ, 778, 172
Perley, D. A., Bloom, J. S., Butler, N. R., et al. 2008, ApJ, 672, 449
Perley, D. A., Cenko, S. B., Bloom, J. S., et al. 2009, AJ, 138, 1690
Perley, D. A., Levan, A. J., Tanvir, N. R., et al. 2013, ApJ, 778, 128
Pilbratt, G. L., Riedinger, J. R., Passvogel, T., et al. 2010, A&A, 518, L1
Poglitsch, A., Waelkens, C., Geis, N., et al. 2010, A&A, 518, L2
Priddey, R. S., Tanvir, N. R., Levan, A. J., et al. 2006, MNRAS, 369, 1189
Prochaska, J. X., Sheffer, Y., Perley, D. A., et al. 2009, ApJ, 691, L27
Rieke, G. H., Young, E. T., Engelbracht, C. W., et al. 2004, ApJS, 154, 25
Robertson, B. E., & Ellis, R. S. 2012, ApJ, 744, 95
Rol, E., van der Horst, A., Wiersema, K., et al. 2007, ApJ, 669, 1098
Rossi, A., Klose, S., Ferrero, P., et al. 2012, A&A, 545, A77
Rossi, A., et al. 2014, A&A, submitted
Roussel, H. 2013, PASP, 125, 1126
Rowlands, K., Dunne, L., Maddox, S., et al. 2012, MNRAS, 419, 2545
Salim, S., Rich, R. M., Charlot, S., et al. 2007, ApJS, 173, 267
Salpeter, E. E. 1955, ApJ, 121, 161
Salvaterra, R., Della Valle, M., Campana, S., et al. 2009, Nature, 461, 1258
Salvaterra, R., Campana, S., Vergani, S. D., et al. 2012, ApJ, 749, 68
Sargent, M. T., Daddi, E., Béthermin, M., et al. 2013, ApJ, submitted [arXiv:1303.4392]
Savaglio, S., Glazebrook, K., & Le Borgne, D. 2009, ApJ, 691, 182
Sawicki, M. 2002, AJ, 124, 3050
Schady, P., Dwelly, T., Page, M. J., et al. 2012, A&A, 537, A15
Schechter, P. 1976, ApJ, 203, 297
Schlegel, D. J., Finkbeiner, D. P., & Davis, M. 1998, ApJ, 500, 525
Shapley, A. E., Erb, D. K., Pettini, M., Steidel, C. C., & Adelberger, K. L. 2004, ApJ, 612, 108
Shapley, A. E., Coil, A. L., Ma, C.-P., & Bundy, K. 2005, ApJ, 635, 1006
Silva, L., Granato, G. L., Bressan, A., & Danese, L. 1998, ApJ, 509, 103
Simpson, C., & Eisenhardt, P. 1999, PASP, 111, 691
Sokolov, V. V., Fatkhullin, T. A., Castro-Tirado, A. J., et al. 2001, A&A, 372, 438
Stanway, E. R., Davies, L. J. M., & Levan, A. J. 2010, MNRAS, 409, L74
Svensson, K. M., Levan, A. J., Tanvir, N. R., et al. 2012, MNRAS, 421, 25
Tanvir, N. R., Barnard, V. E., Blain, A. W., et al. 2004, MNRAS, 352, 1073
Tanvir, N. R., Fox, D. B., Levan, A. J., et al. 2009, Nature, 461, 1254
Tanvir, N. R., Levan, A. J., Fruchter, A. S., et al. 2012, ApJ, 754, 46
Trenti, M., Perna, R., Levesque, E. M., Shull, J. M., & Stocke, J. T. 2012, ApJ, 749, L38
Trenti, M., Perna, R., & Tacchella, S. 2013, ApJ, 773, L22
van der Horst, A. J., Kouveliotou, C., Gehrels, N., et al. 2009, ApJ, 699, 1087
Wanderman, D., & Piran, T. 2010, MNRAS, 406, 1944
Wang, W.-H., Chen, H.-W., & Huang, K.-Y. 2012, ApJ, 761, L32
Wolf, C., & Podsiadlowski, P. 2007, MNRAS, 375, 1049
Woosley, S. E., & Heger, A. 2006, ApJ, 637, 914
Xiao, L., & Schaefer, B. E. 2011, ApJ, 731, 103
Yoldaş, A. K., Krühler, T., Greiner, J., et al. 2008, AIP Conf. Proc., 1000, 227
Yüksel, H., Kistler, M. D., Beacom, J. F., & Hopkins, A. M. 2008, ApJ, 683, L5
Zafar, T., Watson, D., Fynbo, J. P. U., et al. 2011, A&A, 532, A143
Zafar, T., Watson, D., Elíasdóttir, Á., et al. 2012, ApJ, 753, 82

Pages 17 to 19 are available in the electronic edition of the journal at http://www.aanda.org

Appendix A: Photometry tables of the GRBHs

Table A.1. Photometry used in SED fitting.

GRBH	A_V[a] (galactic)	Wavelength (μm)	Flux[b] (μJy)	Uncertainty (μJy)	Reference
(1)	(2)	(3)	(4)	(5)	(6)
970828	0.12	0.640	0.28	0.08	1
		2.160	1.7	0.5	1
		4.501	<3.9	–	This paper
		7.905	10.	4.	This paper
		23.680	44.	2.	This paper
		100.	<7000.	–	This paper
		160.	<15 400.	–	This paper
		250.	<18 900.	–	This paper
		350.	<21 900.	–	This paper
		500.	<29 100.	–	This paper
		865.5	<7080.	–	2
		34 860.	<27.	–	2
980613	0.28	0.434	0.4	0.1	3
		0.545	0.8	0.1	3
		0.640	0.94	0.05	4
		0.760	1.15	0.1	4
		2.214	1.4	0.3	4
		4.501	43.	3.	This paper
		7.905	55.	10.	This paper
		23.680	259.	11.	This paper
		100.	3500.	800.	This paper
		160.	<20 300.	–	This paper
		447.5	<52 800.	–	2
		856.5	<2760.	–	2
980703	0.18	0.445	2.1	0.3	5
		0.557	2.6	0.2	5
		0.639	3.3	0.2	5
		0.801	4.	1.	5
		1.254	7.7	1.	5
		1.651	8.2	2.	5
		2.161	9.6	1.	5
		4.501	6.	2.	This paper
		7.905	<26.	–	This paper
		23.680	70.	3.	This paper
		250.	<20 100.	–	This paper
		350.	<20 400.	–	This paper
		447.5	<32 100.	–	2
		500.	<27 300.	–	This paper
		856.5	<4300.	–	6
		1344.2	<7551.	–	7
		34 700.	39.	4.	7
		62 500.	42.	8.	7
		209 154.	69.	5.	7
990705	0.24	0.545	2.8	0.5	8
		0.640	4.9	0.5	9
		4.501	16.	2.	This paper
		7.905	<16.	–	This paper
		23.680	<58.	–	This paper
		100.	<5800.	–	This paper
		160.	<20 300.	–	This paper
		250.	<19 200.	–	This paper
		350.	<15 600.	–	This paper
		500.	<24 000.	–	This paper
		143 000.	<26.	–	10
020127	0.15	0.480	<0.178	–	11
		0.626	<1.48	–	11
		0.659	0.44	0.06	11
		0.771	1.2	0.1	11
		0.790	0.94	0.09	11
		1.252	11	1	11
		1.253	10	2	This paper
		1.631	20	4	This paper
		2.146	18	6	This paper
		2.162	26	3	11
		3.543	50	1	This paper
		5.711	46	7	This paper
		23.680	160	32	This paper
		100.	<5000	–	This paper
		160.	<17 700	–	This paper
		250.	<17 700	–	This paper
		350.	<21 000	–	This paper
		500.	<18 300	–	This paper
020819B	0.20	0.436	7.	4.	12
		0.459	27.2	0.5	13
		0.622	61.6	3.6	13
		0.660	51.	1.	12
		0.764	83.3	5.2	13
		0.899	117.	2.2	13
		1.240	150.	5.8	13
		1.647	185.	7.7	13
		2.170	150.	15.	13
		3.543	101.	1.	This paper
		4.501	94.	2.	This paper
		5.711	75.	10.	This paper
		7.905	177.	15.	This paper
		23.680	389.	22.	This paper
		100.	19 000.	2000.	This paper
		160.	27 500.	3500.	This paper
		250.	24 000.	12 000.	This paper
		350.	<16 800.	–	This paper
		500.	<24 300.	–	This paper
		30 000.	<138.	–	14
		60 000.	<33.	–	14
030115	0.06	0.435	0.15	0.02	15
		0.606	0.22	0.01	15
		0.814	0.43	0.02	15
		1.100	0.9	0.1	15
		1.600	3.2	0.2	15
		2.200	4.9	0.7	15
		3.543	6.8	0.7	This paper
		4.501	12.0	1.0	This paper
		100.	<3900.	–	This paper
		160.	<18 600.	–	This paper
		450.	<33 000.	–	16
		850.	<2400.	–	16
		1200.	<1800.	–	16

Notes. [(a)] Taken from Schlegel et al. (1998). [(b)] Fluxes corrected for Galactic extinction as given by Col. (2). Flux upper limits are 3σ. [(c)] The position of the host of GRB 060904A was originally associated with a source which had significantly more IRAC 3.6 μm flux than the current photometry. Recently, however, the coordinates were revised making this source fainter than our original sample requirements. We have retained it in our analysis in any case.

References. (1) Djorgovski et al. (2001); (2) Berger et al. (2003); (3) Sokolov et al. (2001); (4) Djorgovski et al. (2003); (5) Christensen et al. (2004); (6) Tanvir et al. (2004); (7) Michałowski et al. (2008); (8) Holland et al. (2000); (9) Bloom et al. (2002); (10) Hatsukade et al. (2012); (11) Berger et al. (2007); (12) Jakobsson et al. (2005); (13) Küpcü Yoldaş et al. (2010); (14) Stanway et al. (2010); (15) Levan et al. (2006); (16) Priddey et al. (2006); (17) http://galex.stsci.edu/GR6/; (18) Rossi et al. (2014); (19) Pellizza et al. (2006); (20) Castro-Tirado et al. (2007); (21) Rol et al. (2007); (22) Perley & Perley (2013); (23) Hjorth et al. (2012); (24) http://www.astro.caltech.edu/grbhosts/; (25) Aoki et al. (2006); (26) Jaunsen et al. (2008); (27) Krühler et al. (2011); (28) Perley et al. (2013); (29) de Ugarte Postigo et al. (2012); (30) Svensson et al. (2012); (31) Hunt et al. (2011); (32) Hashimoto et al. (2010); (33) Holland et al. (2010); (34) http://www.sdss3.org/dr9/; (35) Aoki et al. (2009).

Table A.1. continued.

GRBH	A_V[a] (galactic)	Wavelength (μm)	Flux[b] (μJy)	Uncertainty (μJy)	Reference
(1)	(2)	(3)	(4)	(5)	(6)
050219A	0.51	0.152	<23.	–	17
		0.193	<7.2	–	18
		0.225	<18.9	–	18
		0.227	<21.	–	17
		0.260	<7.4	–	18
		0.347	<8.6	–	18
		0.430	<16.9	–	18
		0.459	16.9	0.6	18
		0.543	28.	3.	18
		0.622	46.	2.0	18
		0.764	65.	2.0	18
		0.899	79.	3.0	18
		1.240	145.	5.0	18
		1.647	179.	17.0	18
		2.170	156.	19.	18
		3.543	85.	2.	This paper
		5.711	58.	8.	This paper
		23.680	19.	5.	This paper
		100.	<5400.	–	This paper
		160.	<15 600.	–	This paper
		250.	<16 500.	–	This paper
		350.	<21 000.	–	This paper
		500.	<24 600.	–	This paper
050223	0.28	0.459	5.9	0.5	This paper
		0.622	9.5	0.6	This paper
		0.660	7.5	0.3	19
		0.764	14.5	1.	This paper
		0.899	9.2	0.9	This paper
		1.256	11.0	2.	This paper
		1.647	12.0	5.	This paper
		2.159	19.3	0.4	19
		3.543	14.1	0.6	This paper
		5.711	11.	3.	This paper
		23.680	16.	4.	This paper
		100.	<4900.	–	This paper
		160.	<21 400.	–	This paper
		250.	<22 200.	–	This paper
		350.	<15 900.	–	This paper
		500.	<25 500.	–	This paper
051022	0.18	0.365	1.7	0.3	20
		0.460	3.7	0.1	20
		0.540	4.9	0.2	21
		0.629	6.3	0.5	21
		0.650	6.14	0.05	21
		0.770	7.66	0.07	21
		0.876	10.5	0.5	21
		0.890	11.6	0.4	21
		1.220	17.7	0.8	21
		1.630	18.	2.	21
		2.159	31.	3.	21
		2.210	29.	1.	21
		3.543	25.	1.	This paper
		4.501	19.	1.	This paper
		100.	6500.	1000.	This paper
		160.	<21 400.	–	This paper
		250.	<17 700.	–	This paper
		350.	<15 600.	–	This paper
		500.	<19 500.	–	This paper
		57 321.7	13.3	3.6	22
		160 000.	<17.	–	10
060904A[c]	0.06	0.547	<0.15	–	24
		0.760	<0.59	–	24
		1.250	<6.6	–	25
		2.160	<5.9	–	25
		3.543	1.5	0.1	This paper
		4.501	2.0	0.2	This paper
		5.711	2.1	0.8	This paper
		7.905	<3.5	–	This paper
		100.	<5000.	–	This paper
		160.	<12 200.	–	This paper

Table A.1. continued.

GRBH	A_V[a] (galactic)	Wavelength (μm)	Flux[b] (μJy)	Uncertainty (μJy)	Reference
(1)	(2)	(3)	(4)	(5)	(6)
070306	0.08	0.352	2.2	0.9	26
		0.459	2.8	0.2	27
		0.622	2.3	0.2	27
		0.655	2.2	0.2	23
		0.764	2.9	0.3	27
		0.790	3.4	0.6	26
		0.899	2.7	0.5	27
		1.240	7.	3.	27
		1.647	10.	3.	27
		2.160	5.7	0.6	23
		3.543	8.7	0.9	This paper
		4.501	15.	2.	This paper
		100.	4900.	700.	This paper
		160.	10 700.	2000.	This paper
071021	0.21	0.550	0.24	0.07	This paper
		0.660	0.17	0.03	This paper
		0.760	0.71	0.14	28
		0.890	0.49	0.16	28
		0.898	0.6	0.3	This paper
		1.230	2.5	1.	This paper
		2.160	5.	1.	This paper
		3.543	12.9	0.7	This paper
		4.501	16.	1.	This paper
		100.	<6000.	–	This paper
		160.	<19 700.	–	This paper
		250.	<19 800.	–	This paper
		350.	<16 200.	–	This paper
		500.	<21 900.	–	This paper
		2860.	<510.	–	29
		3485.	<450.	–	29
		57 321.7	<32.1	–	22
080207	0.07	0.473	0.04	0.01	30
		0.660	0.10	0.4	31
		0.790	0.17	0.05	30
		0.925	0.35	0.05	31
		1.250	1.6	0.3	31
		1.607	2.3	0.4	31
		2.160	7.	1.	31
		3.543	14.4	0.4	31
		4.501	15.5	0.4	31
		5.711	18.5	1.5	31
		7.905	12.5	2.	31
		23.680	92.	7.	31
		100.	2200.	600.	This paper
		160.	5900.	1400.	This paper
		250.	<19 500.	–	This paper
		350.	<20 400.	–	This paper
		449.	<53 220.	–	30
		500.	<21 900.	–	This paper
		825.	<13 120.	–	30
		57 321.7	17.1	2.5	22
080325	0.20	0.450	0.19	0.02	32
		0.660	0.23	0.03	32
		0.780	0.41	0.06	32
		0.918	0.59	0.04	32
		1.199	2.3	0.4	32
		2.198	7.7	0.4	32
		3.543	15.3	0.8	This paper
		4.501	13.9	0.8	This paper
		100.	1400.	400.	This paper
		160.	5000.	800.	This paper
		250.	<18 000.	–	This paper
		350.	<16 800.	–	This paper
		500.	<26 700.	–	This paper
		57 321.7	<15.4	–	22

Table A.1. continued.

GRBH	A_V[a] (Galactic)	Wavelength (μm)	Flux[b] (μJy)	Uncertainty (μJy)	Reference
(1)	(2)	(3)	(4)	(5)	(6)
090404	0.07	0.437	0.02	0.01	28
		0.473	0.14	0.03	28
		0.760	0.19	0.04	28
		1.050	0.29	0.07	28
		1.246	0.59	0.13	28
		1.541	0.95	0.19	28
		2.200	2.44	0.36	28
		3.543	4.	1.	This paper
		4.501	5.	1.	This paper
		100.	<5000.	–	This paper
		160.	<18 200.	–	This paper
		250.	<21 600.	–	This paper
		350.	<22 800.	–	This paper
		500.	<26 100.	–	This paper
		57 321.7	10.9	2.7	22
090417B	0.05	0.193	0.7	0.1	33
		0.225	0.9	0.2	33
		0.260	0.6	0.4	33
		0.347	0.9	0.4	33
		0.431	2.1	0.3	33
		0.477	2.5	0.3	34
		0.623	8.	1.	34
		0.660	9.2	0.3	33
		0.763	10.	1.	34
		0.913	19.	4.	34
		1.250	<16.	–	35
		2.160	<27.	–	35
		3.543	16.	1.	This paper
		4.501	13.	1.	This paper
		100.	1200.	600.	This paper
		160.	3900.	1600.	This paper
		250.	<16 800.	–	This paper
		350.	<19 800.	–	This paper
		500.	<23 400.	–	This paper
		3477.	<510.	–	28
		57 321.7	<21.4	–	22